Breaking of the first adiabatic invariants of charged particles in time-dependent magnetic fields: Computer simulations and theory

Joseph E. Borovsky
Space Plasma Physics Group, Los Alamos National Laboratory, Los Alamos, New Mexico 87545

Paul J. Hansen
Department of Physics and Astronomy, University of Iowa, Iowa City, Iowa 52242

(Received 16 July 1990; revised manuscript received 31 January 1991)

The mechanics of the first adiabatic invariant μ of nonrelativistic charged particles in time-dependent magnetic inductions $B(t)$ are studied by means of computer simulations and analytic theory. Linear-ramp magnetic-induction profiles $B=B_0+(\Delta B/\Delta t)t$ are utilized, as well as hyperbolic-tangent ramps and sine half-wave ramps. The change in μ that results from an induction change ΔB that occurs over a time Δt is quantified for all values of ΔB and Δt, as well as for all values of the particle position. It is found that the cases fall into two categories with very different μ behavior: cases in which the change in the magnetic induction occurs over a time Δt that is *exactly* equal to an integer number of gyroperiods (textbook case) or cases in which the change in the induction occurs over a time Δt that is not equal to an integer number of gyroperiods (more general case). In both categories μ is an adiabatic invariant, although the conservation of μ is much poorer in the latter category. It is pointed out that, in addition to the well-known constraints on ΔB and Δt, there is a constraint on the particle's initial position in the magnetic field if the change in the adiabatic invariant is to be kept small.

I. INTRODUCTION

For a charged particle in nonrelativistic motion in a spatially uniform, temporally varying magnetic field, the quantity

$$\mu=\frac{v_\perp^2}{B} \tag{1}$$

is generally thought to be conserved to a high degree of accuracy provided that

$$\tau_c\frac{dB}{dt}\ll B\ , \tag{2a}$$

$$r_g|\nabla E|\ll E\ , \tag{2b}$$

where $B(T)$ is the magnetic induction, $v_\perp(t)$ is the magnitude of the particle's velocity perpendicular to **B**, $\tau_c(t)=2\pi/(eB/mc)$ is the particle's cyclotron period, $r_g(t)=v_\perp/(eB/mc)$ is the particle's gyroradius, and $E(\mathbf{x},t)$ is the induction electric field that accompanies the time-changing magnetic induction. The quantity μ is known as the first adiabatic invariant of the particle's motion. Nonrelativistically, μ is $2/m$ times the orbital magnetic moment of the particle, where m is the particle's mass. The concept that μ is an invariant for a charged particle is generally attributed to Alfvén,[1] although it was pointed out much earlier by Ehrenfest.[2] The invariance of μ has come to be a fundamental concept of plasma physics,[3,4] space physics,[5,6] and astrophysics.[7,8]

The invariance of μ implies that there is a change in the perpendicular kinetic energy $\frac{1}{2}mv_\perp^2$ of the charged particle when there is a change in the magnetic induction B. This kinetic-energy change (often referred to as betatron acceleration[9,10]) is a result of the work that is done on the cyclotron-orbiting particle by the non-curl-free induction electric field that accompanies the time-changing magnetic induction. The aim of this report is to determine how rugged is the concept of μ being an invariant. The details of the kinetic-energy-change process are examined with the aid of test-particle computer simulations, with emphasis on determining by how much μ changes in a time-changing magnetic field.

The nomenclature used to describe adiabatic invariance will be the following. If $\Delta\mu$ is the change in the value of μ that results from a change ΔB in the value of B that occurs over a time Δt, then μ is adiabatically conserved if[11,12] $\Delta\mu\to 0$ as $\Delta t/\tau_c\to\infty$. For $\tau_c/\Delta t\to 0$, μ is said to be an adiabatic invariant to Nth order in $\tau_c/\Delta t$ if a constant C can be found such that[13]

$$|\Delta\mu|<C\left[\frac{\tau_c}{\Delta t}\right]^N . \tag{3}$$

If μ is an adiabatic invariant to all orders in $\tau_c/\Delta t$, then it is commonly expected that, for $\tau_c/\Delta t\to 0$, the change in μ is related to the time Δt by[14,15] $\Delta\mu\propto e^{-\Delta t/\tau_c}$, where τ_c is the cyclotron period of the particle.

Mathematically, $\mu=v_\perp^2/B$ is shown to be an adiabatic invariant by demonstrating that

$$\frac{d\mu}{dt}=\frac{d}{dt}\left[\frac{1}{\omega_c}\oint v_\perp d\theta\right]=0\ , \tag{4}$$

where θ is the azimuthal angle and where $\oint d\theta=\int_0^{2\pi}d\theta$

denotes that the integral is over exactly a full period of the motion (for example, Eq. 11-135 of Ref. 16 or Eq. 12.64 of Ref. 17). The quantity $\oint v_\perp d\theta$ is the action integral, and as long as the action integral is over a complete period of the motion, it is well known that μ will be an adiabatic invariant.[11,15] For a charged particle performing cyclotron motion, the action integral is complete when Δt is exactly equal to an integer number of gyroperiods.

In this paper, test-particle numerical simulations and analytic theory will be used to study the behavior of charged particles in time-varying magnetic inductions. Cases where Δt is not equal to integer numbers of gyroperiods (incomplete action integrals) are examined, as well as cases where Δt is exactly equal to integer numbers of gyroperiods (complete action integrals). The determination of the fractional change $\Delta\mu/\mu$ of the first adiabatic invariant μ that results from a change in the magnetic induction will be emphasized. Before and after the change, the magnetic induction is constant with time, and it has no spatial gradients. At these times, series expressions for the first adiabatic invariant[18,19] μ that are Taylor expansions in the time derivatives and spatial derivatives of the fields only have their zeroth-order term $v_\perp^2/B$ as nonzero. Therefore, evaluating $v_\perp^2/B$ at these times obtains the full expansion for μ.

The six primary conclusions of this study are the following. Conclusion (1) is that for a given μ value, the change $\Delta\mu$ depends on θ, ΔB, Δt, and x, where θ is the gyrophase angle of the particle about its guiding center, ΔB is the change in the magnetic induction, Δt is the time over which the induction changes, and x is the position of the particle's guiding center with respect to the location in the system where the induction electric field vanishes. The parameters θ and x are defined at some fiducial (initial) time. Thus, conclusion (1) indicates that $\Delta\mu$ depends on the two initial conditions θ and x and on the two parameters of the change ΔB and Δt. Conclusion (2) is that there is a strong oscillation of $\Delta\mu$ as a function of Δt, with $\Delta\mu$ being very small when Δt is exactly equal to integer numbers of gyroperiods (complete action integrals) and $\Delta\mu$ being much larger when Δt is otherwise. Conclusion (3) is that μ is an adiabatic invariant even when Δt is not exactly equal to an integer number of gyroperiods, i.e., that μ is an adiabatic invariant even when the action integrals are incomplete.

Conclusion (4) is that, for cases where Δt is not exactly equal to an integer number of gyroperiods, there is a condition in addition to Eqs. (2) that must be satisfied for $\Delta\mu$ to be small. This third condition is that

$$|\mathbf{x}| \leq r_g \ , \tag{5}$$

where $\mathbf{x}$ is the position of the particle's guiding center relative to the location where the induction electric field vanishes and where r_g is the particle's gyroradius.

Conclusion (5) is that the change $\Delta\mu$ that occurs in cases where Δt is not exactly equal to an integer number of gyroperiods is owed to the excess work that is done during the residual fraction of a gyroperiod after the last completed gyroperiod. Conclusion (6) is that the change $\Delta\mu$ that occurs in cases where Δt is exactly equal to an integer number of gyroperiods is owed to the work done on an orbit that differs from a perfect circle by the following four corrections: (a) the guiding center has an $\mathbf{E}\times\mathbf{B}$ drift, (b) the gyrovelocity changes as B changes, (c) the gyroradius changes as B changes, and (d) the gyrofrequency changes as B changes.

This paper is organized as follows. In Sec. II the mechanics of the adiabatic invariant μ are examined, and the main reason for the failure of μ conservation is discussed. Test-particle simulations that quantify the change $\Delta\mu$ for individual particles and for ensembles of particles are examined in Sec. III. Analytic calculations of the change $\Delta\mu$ are presented in Sec. IV. The adiabatic invariant μ is examined for magnetic-induction ramps $B(t)$ with differing functional forms in Sec. V. Section VI contains a discussion of the literature of μ conservation. Finally, the paper is summarized in Sec. VII.

II. MECHANICS OF THE ADIABATIC INVARIANT μ: THE UNBALANCED WORK PICTURE

When the magnetic induction $\mathbf{B}$ changes with time, a charged particle orbiting in that induction experiences a change in the magnitude of its perpendicular velocity $v_\perp$ because of the work done by a non-curl-free induction electric field $\mathbf{E}$. Taking the magnetic induction to be uniform in space and to point in the $\hat{\mathbf{z}}$ direction, and taking the source currents that produce $\mathbf{B}$ and $\mathbf{E}$ to point only in the $\pm\hat{\mathbf{y}}$ direction, Faraday's law $\partial E_y/\partial x = -(1/c)(\partial B/\partial t)$, yields

$$E_y = -\frac{1}{c}\frac{\partial B}{\partial t}x \ , \tag{6}$$

where the constant of integration was taken to be zero so that $E_y = 0$ at $x = 0$. A positively charged particle orbiting in these fields is depicted in Fig. 1. On the right-hand side of the orbit the particle gains kinetic energy owing to the positive work that is done on it by the induction electric field, and on the left-hand side of its orbit it loses kinetic energy owing to the negative work done there. Because there is a shear in $\mathbf{E}$, the work done on one side of the orbit does not cancel out the work done on the other side; hence there is a net work done on the particle dur-

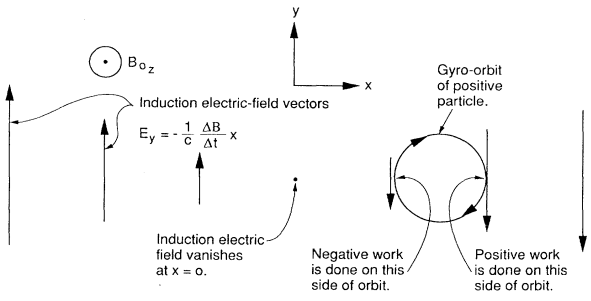

FIG. 1. A sketch of a cyclotron-orbiting particle in a time-dependent magnetic induction with the induction electric field depicted. Note that the orbit's deviation from a circle is not depicted, nor is the $\mathbf{E}\times\mathbf{B}$ drift.

ing a gyroperiod. At the end of every gyroperiod, this work is just the right amount to change $v_\perp^2$ so that μ is very nearly conserved.

The strength of the induction electric field increases with x [as indicated by expression (6)], where x is the position of the particle. If, in Fig. 1, the particle were located a very large distance from $x=0$, then the amount of work done on the right-hand side of its orbit and the amount of work done on the left-hand side of its orbit would both be very large; yet, because the gradient in the induction electric field E_y does not vary in space, the difference between the two amounts would still be just that needed to very nearly conserve μ each gyroperiod.

However, μ conservation is poor if the gyro-orbits are incomplete. If, in Fig. 1, the particle starts at the top of its orbit and the magnetic-field change occurs over $3\frac{1}{4}$ gyroperiods τ_c, then μ will be well conserved at times $t=1\tau_c$, $t=2\tau_c$, and $t=3\tau_c$, but from time $t=3\tau_c$ to $t=3\frac{1}{4}\tau_c$ the work on the particle by the electric field is only positive. Hence, the work done on the particle during the final $\frac{1}{4}$ orbit is not balanced by the work done during another portion of the orbit. Therefore, at the end of this $3\frac{1}{4}$ gyro-orbits, μ will not be well conserved. In general, a change in the magnetic induction will not occur exactly over an integer number of gyroperiods; rather the change will end with a fraction of a gyroperiod left over. The conservation of μ is worse the further the particle is from $x=0$. This is because the strength of the induction electric field increases linearly with x away from $x=0$ and therefore the unbalanced work done on the particle increases with x.

The parameters that $\Delta\mu$ depends on can be determined by means of this unbalanced work picture. For a magnetic induction $B(t)$ that varies linearly with time, the magnetic induction $\mathbf{B}=B\hat{\mathbf{z}}$ goes from the value B_0 to the value $B_0+\Delta B$ in a time Δt:

$$B=\begin{cases} B_0, & t\le 0 \\ B_0+\dfrac{\Delta B}{\Delta t}t, & 0\le t\le \Delta t \\ B_0+\Delta B, & t\ge \Delta t \ . \end{cases} \tag{7}$$

This spatially homogeneous, linearly time-varying magnetic induction has an induction electric field accompanying it for $0\le t\le\Delta t$ given by [from relation (6)]

$$E_y=-\frac{1}{c}\frac{\Delta B}{\Delta t}x \ . \tag{8}$$

The effect of this unbalanced fraction of a gyroperiod on μ is estimated as follows. During an unbalanced $\frac{1}{2}$ of a gyroperiod, the magnetic induction changes by an amount $\delta B=\Delta B(\frac{1}{2}\tau_c/\Delta t)$, where τ_c is the gyroperiod during the change in B. During this time the perpendicular velocity of a particle changes by

$$\delta v_\perp\sim(e/m)E_y\delta t=\omega_c(\Delta B/B)x(\tfrac{1}{2}\tau_c/\Delta t) \ .$$

From Eq. (1), the change $\Delta\mu$ in the adiabatic invariant μ can be written $(\Delta\mu/\mu)=2(\delta v_\perp/v_\perp)-(\delta B/B)$; using the above expressions for δB and $\delta v_\perp$, this becomes

$$\frac{\Delta\mu}{\mu}\simeq\frac{\Delta B}{B}\frac{\tau_c}{\Delta t}\left[\frac{x}{r_g}-\frac{1}{2}\right] \ . \tag{9}$$

As can be seen in expression (9), there are three physical parameters that determine the change in μ during the residual fraction of a gyroperiod: $\Delta B/B$, which is the fractional change in the magnetic induction; $\Delta t/\tau_c$, which is the time over which the magnetic induction changes relative to the cyclotron period; and x/r_g, which is the distance of the particle from the $x=0$ plane relative to the particle's gyroradius. When test-particle simulations are performed to study $\Delta\mu$, these three quantities will be varied.

III. TEST-PARTICLE SIMULATIONS OF μ BREAKING

The change in the adiabatic invariant of a particle is investigated by numerically solving the nonrelativistic equations of motion

$$\frac{d\mathbf{v}}{dt}=\frac{q}{m}\mathbf{E}+\frac{q}{mc}\mathbf{v}\times\mathbf{B} \ , \tag{10a}$$

$$\frac{d\mathbf{x}}{dt}=\mathbf{v} \tag{10b}$$

for that particle in the magnetic-induction $\mathbf{B}$ and induction electric field $\mathbf{E}$ as given by Eqs. (7) and (8). Equations (10a) and (10b) are solved with a simple first-order, time-centered numerical scheme in double precision. Typically, 1×10^4 to 2×10^8 time steps are used per gyroperiod, and the simulations are accurate to about 1 part in 10^8 in determining $\Delta\mu/\mu$. The orbits for ensembles of particles are calculated, the particles in an ensemble all having the same mass, the same charge, the same initial guiding-center position, and the same initial value of $|v_\perp|$ before the change in B, but having differing initial gyrophase angles θ_0. The initial x, y, v_x, and v_y values are given by

$$x=x_{gc0}+r_{g0}\cos(\theta_0) \ , \tag{11a}$$

$$y=y_{gc0}-r_{g0}\sin(\theta_0) \ , \tag{11b}$$

$$v_x=-v_{\perp0}\sin(\theta_0) \ , \tag{11c}$$

$$v_y=-v_{\perp0}\cos(\theta_0) \ , \tag{11d}$$

where (x_{gc0},y_{gc0}) are the coordinates of the guiding center at time $t=0$ and $r_{g0}=v_{\perp0}/\omega_{c0}$ and $v_{\perp0}$ are the gyroradius and perpendicular velocity of the particles at $t=0$. The gyrophase angle θ is measured counterclockwise from the x axis in Fig. 1. In the ensembles, the particles are equally spaced in gyrophase angle; hence ensemble averaging is equivalent to gyrophase averaging. In this report, all of the ensembles contain 500 particles, except for the simulations of Sec. III C, where the ensembles contain 1500 particles. For each particle, the quantity $\Delta\mu=\mu_{\text{final}}-\mu_0$ is measured, where μ_0 is the first adiabatic invariant before the induction change and μ_{final} is its value after the induction change. For each set (ensemble) of particle orbits, the following three quantities are extracted: The gyrophase average (first moment) of $\Delta\mu$

$$\langle \Delta\mu \rangle = \frac{\sum_{j=1}^{500} (\Delta\mu)_j}{500} , \tag{12}$$

the standard deviation (second moment) of $\Delta\mu$

$$\sigma(\Delta\mu) = \langle (\Delta\mu - \langle \Delta\mu \rangle)^2 \rangle^{1/2} = \left[\frac{\sum_{j=1}^{500} [(\Delta\mu)_j - \langle \Delta\mu \rangle]^2}{500} \right]^{1/2} , \tag{13}$$

and the maximum of the 500 values of $|\Delta\mu|$, denoted as $\Delta\mu_{\max}$. For all of the results presented in this report, the ensemble-averaged quantities are not found to change perceptibly if the size of the ensembles are increased.

The discussion of the test-particle simulations is divided up into four subsections. In Sec. III A some properties of particle orbits will be discussed. In Sec. III B measurements of $\Delta\mu/\mu$ and its ensemble averages will be presented for cases where Δt does not equal integer numbers of gyroperiods and expressions for $\Delta\mu(\Delta B, \Delta t, x_0)$ when Δt is unequal to integer numbers of gyroperiods will be determined. Finally, in Sec. III C, orbit calculations for ensembles of particles are performed for cases where Δt is exactly equal to integer numbers of gyroperiods and expressions for $\Delta\mu(\Delta B, \Delta t, x_{g0})$ are obtained from these simulations results.

A. Properties of the particle orbits

There are three things to note in the orbit of a charged particle in a time-changing magnetic induction. First there is the familiar contraction or expansion of the particle's gyro-orbit accompanied by the changes in the gyrovelocity and gyrofrequency. Additionally, there is a shift in the particle's guiding center in the $\mathbf{E}\times\mathbf{B}$ direction (x direction), where $\mathbf{E}$ is the induction electric field. Finally, there is a subtle shift of the guiding center in the direction (y direction) normal to both $\mathbf{B}$ and $\mathbf{E}\times\mathbf{B}$.

The major portion of the x shift of the guiding centers is the shift that is obtained by integrating the $\mathbf{E}\times\mathbf{B}$ drift velocity evaluated at the guiding center, as follows. For the $\mathbf{E}\times\mathbf{B}$ drift, the time rate of change of x_{gc} is $dx_{gc}/dt = cE_y/B$. With B given by expression (7) and E_y given by expression (8), evaluating this expression at $x = x_{gc}$ gives

$$\frac{dx_{gc}}{dt} = -\frac{\Delta B}{\Delta t} \frac{x_{gc}}{B_0 + \left[\frac{\Delta B}{\Delta t} \right] t} ,$$

which can be integrated $\int_0^{\Delta t} dt$ and $\int_{x_{gc0}}^{x_{gc}} dx_{gc}$ to yield

$$x_{gc} = x_{gc0} \frac{B_0}{B_0 + \Delta B} , \tag{14}$$

where x_{gc0} is the x position of the particle's guiding center before the change in magnetic induction. This shift is independent of the initial gyrophase angle θ_0 of a particle and it is independent of μ and Δt. The $\mathbf{E}\times\mathbf{B}$ drift guiding-center shift leads to a convergence or divergence of the particle orbits toward or away from the $x = 0$ plane depending on whether B is increasing or decreasing with time. Another way to picture this x shift is to say that the particles are carried by the lines of flux (see, for example, Sec. 5.4 of Ref. 20), which move in toward or away from the $x = 0$ plane to produce the increase or decrease in B. The shift expressed by Eq. (14) matches the x shift of the guiding centers of the computer-simulated particles very well, although the guiding centers in the simulation are found to move slightly faster than this $\mathbf{E}\times\mathbf{B}$ drift predicts, leading to a slight overconvergence toward $x = 0$ or a slight overdivergence away from $x = 0$

The guiding-center shifts Δy that the particles obtain in the y direction are strongly dependent on the initial gyrophase angles θ_0 of the particles, unlike the Δx shift. The shift Δy has a sinusoidal dependence on θ_0 (with one period per 360° of θ_0) with the sinusoid centered on $\Delta y \cong 0$. The gyrophase average of Δy is small, but it is nonzero. For a positive particle, when the magnetic induction increases ($\Delta B > 0$) the gyrophase average $\langle \Delta y \rangle$ is in the direction of the local induction electric field, but when the magnetic induction decreases ($\Delta B < 0$), the average (Δy) is in the opposite direction to the local induction electric field. In both cases the gyrophase average $\langle \Delta\mu \rangle$ is positive; this means that the value of $\langle \Delta\mu \rangle$ cannot be estimated by calculating the work $q\langle \mathbf{E}\cdot\Delta\mathbf{y} \rangle$ done on the mean guiding-center position, which moves a distance of $\langle \Delta y \rangle$ in the induction electric field. For both $\Delta B/B_0$ large or small, $\langle \Delta y \rangle / r_{g0} \propto (\Delta t/\tau_{c0})^{-1}$ for $\Delta t > \tau_{c0}$ with some dependence on the phase of the gyroperiod.

In Fig. 2 the fractional change in the quantity $\mu = v_\perp^2/B$ is explored as a function of the particle's initial gyrophase angle θ_0. In each panel of the figure, orbits were calculated for 360 particles evenly spaced in θ_0 for $0° \le \theta_0 \le 360°$. The change in the adiabatic invariant $\Delta\mu$ of a particle caused by the change in induction ΔB is strongly dependent on the initial gyrophase angle θ_0 of that particle. In the top panel, particles with $\theta_0 \cong 270°$ gain the most energy and particles with $\theta_0 \cong 90°$ lose the most energy. This fits well with the unbalanced work picture described in Sec. II, wherein the excess work done on a particle can be positive or negative depending on whether it moves with or against the induction electric field on the final unbalanced portion of its gyro-orbit. Averaging the $\Delta\mu$ values of the particles over the initial gyrophase angles θ_0, it is found that this averaged quantity $\langle \Delta\mu \rangle$ is much less than a typical $|\Delta\mu|$. Note also that the $\Delta\mu$ versus θ_0 phase relationships are quite different for $|x_{gc0}| < |r_{g0}$ than for $|x_{gc0}| > r_{g0}$. This is because for $|x_{gc0}| < r_{g0}$ particles in the ensemble initially lie on both sides of the $x = 0$ plane, and so both positively directed and negatively directed E_y are sampled by the ensemble (see, for example, Fig. 1). Accordingly, there are now two regions on the gyrocircle where positive work can be done, and hence there are two peaks in the $\Delta\mu$ versus θ_0 phase relations. Because of this, the details of μ breaking are different for $|x_{gc0}| < r_{g0}$ than for $|x_{gc0}| > r_{g0}$. As can be seen in Fig. 2, the $\Delta\mu$ versus θ_0 phase relations are reversed for $x_0 > 0$ and $x_0 < 0$; this is to be expected from the unbalanced work picture, because the sign of the in-

duction electric field is reversed for $x_0>0$ and $x_0<0$. Thus, for a given gyrophase position, positive work becomes negative work and vice versa. The $\Delta\mu$ versus θ_0 phase relations are invariant to the sign of the charged particle and $\Delta\mu$ changes sign in the $\Delta\mu$ versus θ_0 phase relations when ΔB is negative instead of positive.

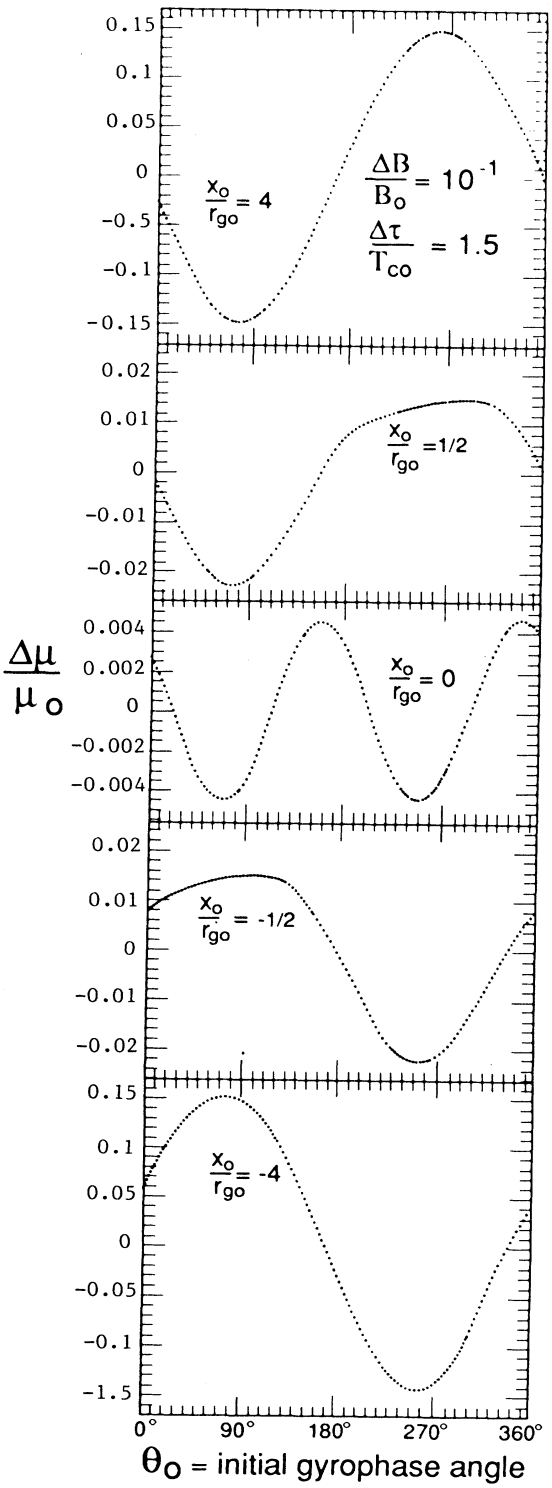

FIG. 2. For five different values of x_0/r_{g0}, the fractional change in the magnetic moment μ of 360 charged particles is plotted as a function of their initial gyrophase angle.

B. Measurements of $\Delta\mu$ for arbitrary Δt values

In this subsection, measurements of the change $\Delta\mu$ in the first adiabatic invariant $\mu=v_\perp^2/B$ associated with a change in the magnetic induction B are obtained by test-particle computer simulations. Four quantities are separately varied in the simulations: the change ΔB in the magnetic induction, the time Δt over which the magnetic induction changes, the initial distance x_{g0} of the particles' guiding centers from the location where the induction electric field vanishes, and the initial gyrovelocity $v_{\perp 0}$ of the particles. The quantities B_0, m, and e will be held constant for all of the simulations. Plots of the two moments $\langle\Delta\mu\rangle$ and $\sigma(\Delta\mu)$ and of $\Delta\mu|_{\max}$ versus these four quantities are presented, with 500 orbits being calculated for each data point.

In Fig. 3 the gyrophase-averaged quantity $\langle\Delta\mu\rangle$ is plotted as a function of time during a change in B for four different values of dB/dt. Clearly, as dB/dt increases, $\langle\Delta\mu\rangle$ increases. There is also a periodic dependence of $\langle\Delta\mu\rangle$ on t. On the top curve, and to a lesser extent on the second curve, the amplitude of the periodic variation in $\langle\Delta\mu\rangle$ decreases with time and the period of the variation decreases with time. The period decreasing with time is simply caused by the fact that the gyroperiod decreases with time as the induction increases. The amplitude decrease originates from the fact that $v_\perp^2$ oscillates at a constant amplitude while B steadily increases; hence $\mu=v_\perp^2/B$ has a decreasing oscillation amplitude. Note that the minima in the temporal oscillations are not fully resolved.

In Fig. 4 the three quantities $\langle\Delta\mu\rangle/\mu_0$, $\sigma(\Delta\mu)/\mu_0$, and $\Delta\mu_{\max}/\mu_0$ are plotted as functions of the magnetic-induction-change time Δt for fixed values of ΔB, x_0, and $v_{\perp 0}$. Three things should be noticed in the graph. The first is that there is a periodic oscillation in $\Delta\mu$ versus Δt with $\Delta\mu$ being very small at the end of every gyroperiod. This fits with the picture of adiabatic-invariant breaking being owed to the unbalanced work done on the particles: At the end of each gyroperiod, the gyro-orbits are complete, the work is balanced, and μ is better conserved; for values of Δt that are not exactly equal to integer numbers of gyroperiods, the work is not balanced because the gyro-orbits are incomplete and hence μ is not so well conserved. While the magnetic induction is changing, $B=B_0+(\Delta B/\Delta t)t$, the gyrophase of a particle changes according to $d\theta/dt=\omega_c(t)=eB(t)/mc$, which may be integrated to obtain

$$\theta=\omega_{c0}t[1+\tfrac{1}{2}(\Delta B/B_0)(t/\Delta t)]+\theta_0 .$$

Accordingly, the ramp period Δt will correspond to the completion of the Nth gyroperiod ($\theta-\theta_0=N2\pi$) when

$$\Delta t=\frac{N\tau_{c0}}{1+\frac{1}{2}\Delta B/B_0} , \tag{15}$$

where $N=1,2,3,\ldots$ is an integer and where τ_{c0} is the gyroperiod before the induction change. Equation (15)

precisely describes the Δt values of the minima in Fig. 4. (Note that the depths of these minima are not resolved in the plot.) The second item to be noticed in Fig. 4 is that $\langle \Delta\mu \rangle \ll \sigma(\Delta\mu)$ for Δt large; i.e., the spread in the $\Delta\mu$ values for the ensemble of orbits is much greater than the mean value of $\Delta\mu$. The third item to be noticed in Fig. 4 is that $\Delta\mu \neq -\Delta B/(B_0+\Delta B)$ for $\Delta t \to 0$. This indicates that the kinetic energy of a particle does not remain constant as the magnetic induction changes infinitely fast, as might naively be thought. Rather, the induction electric field during the rapid change in B gives a strong impulsive kick to the particles and changes their kinetic energies.

In Fig. 5, $\langle \Delta\mu \rangle/\mu_0$ is plotted as a function of the change time Δt of the linear-ramp induction variation for four sets of particles: a set with guiding centers initially located at $x_{g0}/r_{g_{g0}}=6$, a set with $x_{g0}/r_{g_{g0}}=4$, a set with $x_{g0}/r_{g_{g0}}=2$, and a set with $x_{g0}/r_{g_{g0}}=0$, where x_{g0} is the distance from the point where the guiding center of the particles initially resides to the plane where the induction electric field vanishes. Note that for x_{g0} increasing, the

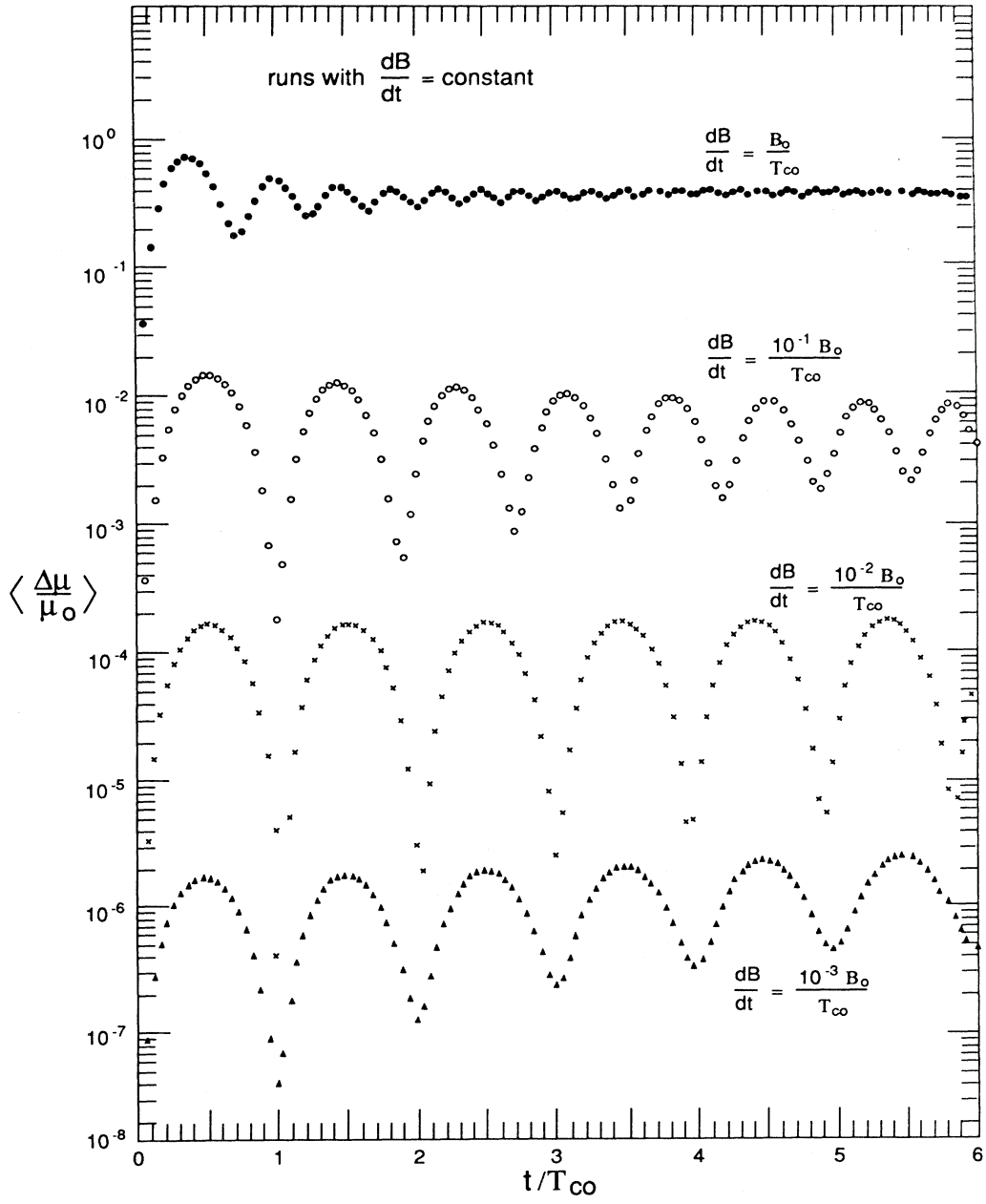

FIG. 3. For ensembles of 500 test particles, $(\Delta\mu)/\mu_0$ is plotted as a function of t/τ_{c0} for four values of dB/dt.

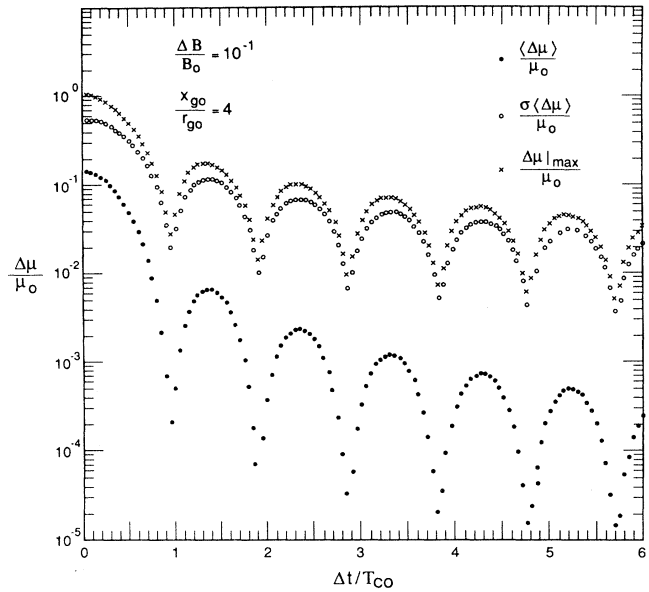

FIG. 4. For ensembles of 500 test particles, the quantities $\langle \Delta\mu \rangle / \mu_0$, $\sigma(\Delta\mu)/\mu_0$, and $\Delta\mu|_{\max}/\mu_0$ are plotted as functions of $\Delta t/\tau_{c0}$.

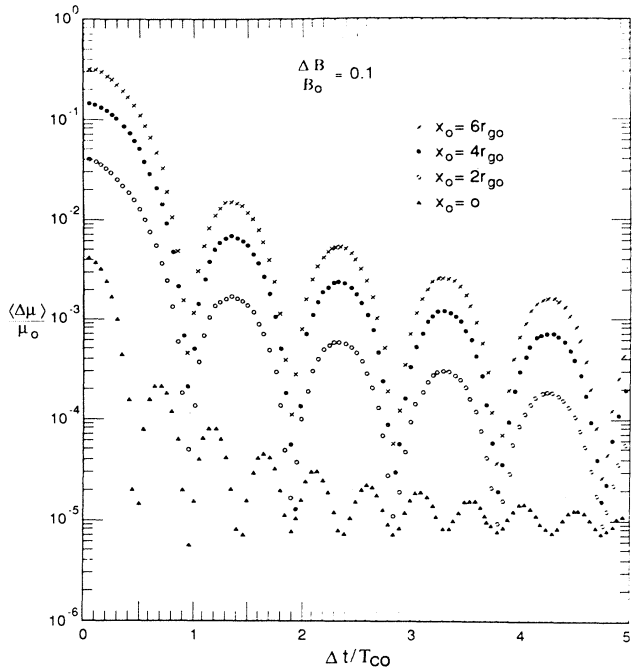

FIG. 5. For ensembles of 500 test particles, $\langle \Delta\mu \rangle / \mu_0$ is plotted as a function of $\Delta t/\tau_{c0}$ for four values of x_0/r_{g0}.

degree of μ breaking increases. This agrees with the unbalanced work picture wherein, because the strength of the induction electric field increases with x, the size of the unbalanced work increases with x, so $\Delta\mu$ increases with x. Examining the three sets of particles with $x_{g0}/r_{g_0} > 1$, it is evident that there is a periodicity to $\langle \Delta\mu \rangle$, with $\langle \Delta\mu \rangle$ being smallest whenever Δt satisfies condition (15). In contrast, for the $|x_{g0}| = 0$ points there is a periodicity of $\frac{1}{2}\tau_c$ to $\Delta\mu$ versus Δt. The differing periodicities are explained with the use of Fig. 1. When the particle's guiding center is located at $|x_{g0}| > r_{g0}$, the work done on the side of the particle's orbit farthest from $x = 0$ is positive and the work done on the side nearest to $x = 0$ is negative, and the difference between these two amounts of work is just enough to change the particle's kinetic energy so that μ is nearly conserved once per gyroperiod. Now imagining an orbit with its gyrocenter located at $x = 0$ in Fig. 1, the work on the gyrating particle by the electric field is always positive. However, the rate of doing work is greatest at $x = x_{\max}$ and $x = x_{\min}$ (rightmost and leftmost points) where $\mathbf{v}\cdot\mathbf{E}$ is greatest and the rate of doing work is zero at the two $x = 0$ points (top and bottom); the work done on the particle near the right and left extrema of the orbit exceeds the work needed to preserve μ, and the work done near the top and bottom of the orbit is less than the work required to preserve μ. Whenever half of an orbit is completed, the work totals that required to nearly conserve μ; hence, the double periodicity to the $x_{g0} = 0$ curve. This is also related to the doubling of the periodicity in Fig. 2.

In Fig. 6 the three ensemble quantities $\langle \Delta\mu \rangle$, $\sigma(\Delta\mu)$, and $\Delta\mu|_{\max}$ are plotted as functions of ΔB for fixed values of x_{g0}, $v_{\perp g0}$, and Δt. In the left-hand panel $\Delta B < 0$ (the magnetic induction decreases in the ramp), and in the right-hand panel $\Delta B > 0$ (the induction increases in the ramp). The curves are fairly straight, with two exceptions. The first irregularity occurs in the left-hand panel; as $\Delta B \to -B_0$ the curves turn sharply upward. In fact, $\Delta\mu \to \infty$ as $\Delta B \to -B_0$. This is caused by the fact that as $\Delta B \to -\Delta B$, $B \to 0$ in the denominator of $\mu = v_\perp^2/B$, while $v_\perp^2$ does not go to zero in the numerator (see, for example, Ref. 21). The second irregularity occurs in the right-hand panel where the straight curves become wavy at $\Delta B \sim B_0$. The cause of these ripples is that when the ramp time Δt is held fixed, the number of gyroperiods in the ramp is not fixed because the induction B changes appreciably [see expression (15)]. This means that some of the $\Delta\mu/\mu_0$ versus $\Delta t/\tau_{c0}$ structure that was seen in Fig. 5 is being introduced into Fig. 6 at high-ΔB values, hence the waviness. For small ΔB values, the curves of Fig. 6 can be fit by straight lines. For $|\Delta B| \ll B_0$, the computer data are very well described by $\langle \Delta\mu \rangle \propto (\Delta B)^2$ and $\sigma(\Delta\mu) \propto (|\Delta B|)^1$ for fixed x_{g0}, $v_{\perp g0}$, and Δt. (Note that μ_0 does not vary with ΔB, which allowed the $\Delta\mu$ scalings to be directly extracted from the plots of $\Delta\mu/\mu_0$).

In Fig. 7 the change $\Delta\mu$ is plotted versus x_{g0}, the initial distance of the guiding center from the $x = 0$ plane, with ΔB, Δt, and $v_{\perp 0}$ held constant. Note that holding $v_{\perp 0}$ constant holds r_{g0} constant and μ_0 constant because B_0 is constant. As can be seen in the figure, there are two distinct regions: $x_{g0} > r_{g0}$ and $x_{g0} < r_{g0}$. In the $x_{g0}/r_{g0} \geq 1$ region the curves are well described by $\langle \Delta\mu \rangle \propto x_{g0}^2$ and $\sigma(\Delta\mu) \propto |x_{g0}|^1$. (Note that these scalings are not limited to $\Delta\mu/\mu_0$ being small.) In Fig. 7, as $x_{g0} \to 0$, the $\Delta\mu$ quantities lose their dependence on x_{g0}. The limiting values are not computational artifacts: Increasing the accuracy of the orbit calculations and increasing the num-

ber of orbits used for the ensemble averages do not change the limiting values. In the $x_{g0} \ll r_{g0}$ regime, the scalings are $\langle \Delta\mu \rangle \propto x_{g0}^0$, $\sigma(\Delta\mu) \propto x_{g0}^0$, and $\Delta\mu|_{\max} \propto x_{g0}^0$. As can be seen from Fig. 7, as x_{g0} increases, the degree of μ breaking increases. Thus, even though $\Delta B/B_0$ is small, $\Delta t/\tau_{c0}$ is large, and the gradients in the electromagnetic fields are weak on gyroradius spacial scales, $\Delta\mu/\mu_0$ can become large if x_{g0}/r_{g0} becomes large.

In Fig. 8 $\Delta\mu$ is plotted versus $v_{\perp 0}$, the initial gyrovelocity of the particles, with ΔB, Δt, and x_{g0} held constant. Clearly there are two distinct regimes: $v_{\perp 0} \leq x_{g0}\omega_{c0}$ and $v_{\perp 0} \gg x_{g0}\omega_{c0}$. This is not surprising since $v_{\perp 0}/x_{g0}\omega_{c0}$ is simply $(x_{g0}/r_{g0})^{-1}$ and since the $\Delta\mu$ versus x_{g0}/r_{g0} plots of Fig. 7 exhibited two distinct regimes. In Fig. 8, when $v_{\perp 0}$ varies, μ_0 also varies. In the $v_{\perp 0} < x_{g0}\omega_{c0}$ regime (which is $x_0 > r_{g0}$), the curves of Fig. 8 are well described by $\langle \Delta\mu \rangle/\mu_0 \propto v_{\perp 0}^{-2}$ and $\sigma(\Delta\mu)/\mu_0 \propto v_{\perp 0}^{-1}$. Since $\mu_0 \propto v_{\perp 0}^2$ (for B_0 fixed), these scalings can be rewritten $\langle \Delta\mu \rangle \propto v_{\perp 0}^0$ and $\sigma(\Delta\mu) \propto v_{\perp 0}^1$. The $\sigma(\Delta\mu)$ scaling makes sense in terms of the unbalanced-work picture presented in Sec. II. In that picture the standard deviation $\sigma(\Delta\mu)$ is a measure of the spread of the work done on the particles about their guiding center. The work done on a particle by an electric field depends on the distance that the particle moves through the field. A particle can move about two gyroradii through the field, hence these individual amounts of work depend linearly on the size of the gyroorbits. Since $r_{g0} \cong v_{\perp 0}/\omega_{c0}$, this yields a $v_{\perp 0}^1$ dependence on the individual $\Delta\mu$ values; hence $\sigma(\Delta\mu) \propto v_{\perp 0}^1$. In the $v_{\perp 0} \gg x_{g0}\omega_{c0}$ regime (which is $x_{g0} \ll r_{g0}$), the scalings exhibited in Fig. 8 are $\langle \Delta\mu \rangle/\mu_0 \propto v_{\perp 0}^0$ and $\sigma(\Delta\mu)/\mu_0 \propto v_{\perp 0}^0$. Again using the fact that $\mu_0 \propto v_{\perp 0}^2$ (for fixed B_0), these scalings yield $\langle \Delta\mu \rangle \propto v_{\perp 0}^2$ and $\sigma(\Delta\mu) \propto v_{\perp 0}^2$. In terms of the unbalanced-work picture, the $\sigma(\Delta\mu)$ scaling for $v_{\perp 0} \gg x_{g0}\omega_{c0}$ makes sense as follows. The quantity $\sigma(\Delta\mu)$ is a measure of the work done on an individual particle. For a particle with its guiding center on the origin, the strength of the induction electric field that it samples is proportional to its gyroradius [see Eq. (8)], and the distance that the particle moves in the electric field is also proportional to its gyroradius, hence the work is proportional to r_{g0}^2, which means that it is proportional to $v_{\perp 0}^2$; hence the $\sigma(\Delta\mu) \propto v_{\perp 0}^2$ scaling. Recall from Fig. 5 that there are periodicities of $\Delta\mu$ versus Δt: If Δt were to be varied, then the $v_{\perp 0} < x_{g0}\omega_{co}$ portions of the curves of Fig. 8 would move up and down with period τ_c keeping the same slope, and the $v_{\perp 0} \gg x_{g0}\omega_{c0}$ portions of the curves would move up and down with period $\frac{1}{2}\tau_c$.

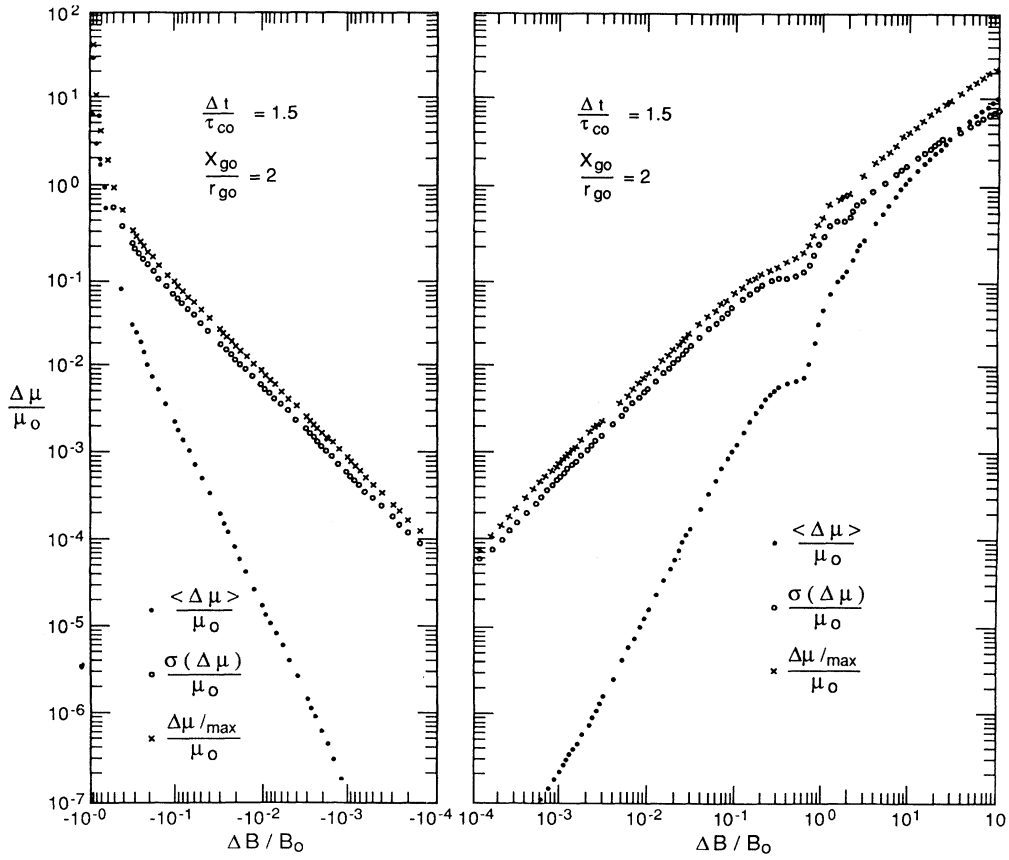

FIG. 6. For ensembles of 500 test particles, the quantities $\langle \Delta\mu \rangle/\mu_0$, $\sigma(\Delta\mu)/\mu_0$, and $\Delta\mu|_{\max}/\mu_0$ are plotted as functions of $\Delta B/B_0$. In the left panel B decreases, and in the right panel B increases.

The final computer-simulation graph of this subsection is Fig. 9, which contains $\Delta\mu/\mu_0$ plotted versus $\Delta t/\tau_{c0}$ at peaks in the $\Delta\mu$ versus Δt oscillations (see Fig. 4). The Δt values at which these peaks occur are $\Delta t=(N-\frac{1}{2})\tau_{c0}/[1+\frac{1}{2}(\Delta B/B_0)]$. The quantities $\langle\Delta\mu\rangle$, $\sigma(\Delta\mu)$, and $\Delta\mu|_{\max}$ are displayed for two different values of $\Delta B/B_0$. The top curves are for $\Delta B/B_0=10^1$, and the bottom curves are for $\Delta B/B_0=10^{-2}$. Noting that μ_0 and τ_{c0} are independent of Δt, the curves of Fig. 9 are well described by $\langle\Delta\mu\rangle\propto\Delta t^{-2}$ and $\sigma(\Delta\mu)\propto\Delta t^{-1}$. These scalings hold for $\Delta B>B_0$ as well as for $\Delta B<B_0$. The scalings also hold for $x_{g0}<r_{g0}$, although no such data are displayed in the figure. In the unbalanced-work picture the $\sigma(\Delta\mu)$ scaling makes sense as follows. The standard deviation $\sigma(\Delta\mu)$ is a measure of the work done on an individual particle as it moves about its guiding center, and this work depends linearly on the induction electric field E_y and on the size of the gyro-orbit. The size of the gyro-orbit is independent of Δt and $E_y\propto\Delta t^{-1}$ [see expression (8)]. Therefore the work (and so $\Delta\mu$) is proportional to Δt^{-1}. This gives the $\sigma(\Delta\mu)\propto\Delta t^{-1}$ scaling.

The scaling relations obtained from Figs. 6–9 can be combined to obtain expressions for $\langle\Delta\mu\rangle$ and $\sigma(\Delta\mu)$ as functions of ΔB, Δt, x_{g0}, and $v_{\perp 0}$ for cases where Δt is not

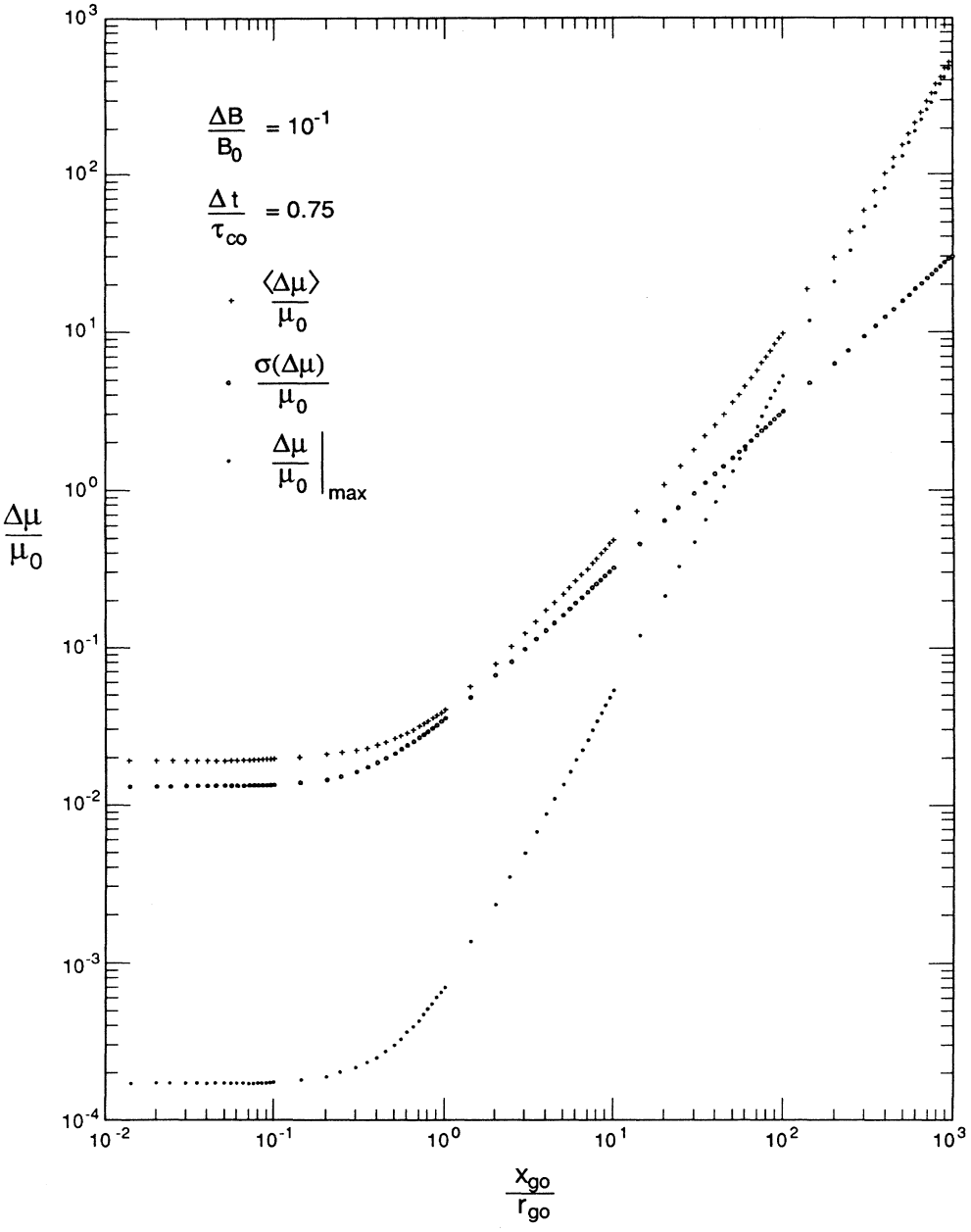

FIG. 7. For ensembles of 500 test particles, the quantities $\langle\Delta\mu\rangle/\mu_0$, $\sigma(\Delta\mu)/\mu_0$, and $\Delta\mu|_{\max}/\mu_0$ are plotted as functions of x_0/r_{g0}.

equal to an integer number of gyroperiods. As noted in Sec. III B, there are two distinct regimes for the $\Delta\mu$ results: $x_{g0} > r_{g0}$ and $x_{g0} < r_{g0}$. Separate fits to the data will be made in both regimes.

For the $x_{g0} \geq r_{g0}$ regime, the scaling relations combine to yield $\langle\Delta\mu\rangle \propto \Delta B^2 x_{g0}^2 v_{\perp 0}^0 \Delta t^{-2}$ and $\sigma(\Delta\mu) \propto \Delta B^0 x_{g0}^0 v_{\perp 0}^1 \Delta t^{-1}$. Dividing these relations by $\mu_0 = v_{\perp 0}^2 / B_0$, using $\tau_{c0} = 2\pi/\omega_{c0}$ and $r_{g0} = v_{\perp 0}/\omega_{c0}$, and introducing the constants C_1 and C_2 to replace the $\propto$ signs, these become

$$\langle\Delta\mu\rangle/\mu_0 = C_1(\Delta B/B_0)^2(x_{g0}/r_{g0})^2(\tau_{c0}/\Delta t)^2$$

and

$$\sigma(\Delta\mu)/\mu_0 = C_2(|\Delta B|/B_0)^1(|x_{g0}|/r_{g0})^1(\tau_{c0}/\Delta t)^1 .$$

The constants C_1 and C_2 can be determined with two data points. Data from Fig. 9 are used: $\langle\Delta\mu\rangle/\mu_0 = 4.4886\times10^{-4}$ and $\sigma(\Delta\mu)/\mu_0 = 2.9935\times10^{-2}$ for $\Delta B/B_0 = 1.000\times10^{-2}$, $\Delta t/\tau_{c0} = 1.4286$, and $x_{g0}/r_{g0} = 1.000\times10^{1}$. These yield $C_1 \cong 9.160\times10^{-2}$ and $C_2 \cong 4.276\times10^{-1}$. Thus, for $x_{g0} \geq r_{g0}$,

$$\frac{\langle\Delta\mu\rangle}{\mu_0} = 9.160\times10^{-2}\left[\frac{\Delta B}{B_0}\right]^2\left[\frac{x_{g0}}{r_{g0}}\right]^2\left[\frac{\tau_{c0}}{\Delta t}\right]^2, \quad (16a)$$

$$\frac{\sigma(\Delta\mu)}{\mu_0} = 4.276\times10^{-1}\left[\frac{|\Delta B|}{B_0}\right]^1\left[\frac{|x_{g0}|}{r_{g0}}\right]^1\left[\frac{\tau_{c0}}{\Delta t}\right]^1, \quad (16b)$$

which holds at the peaks of the $\Delta\mu$ versus Δt oscillations. Expressions (16) are valid for $\Delta t \geq 1.5\tau_{c0}, \Delta B \leq 10^{-1} B_0$,

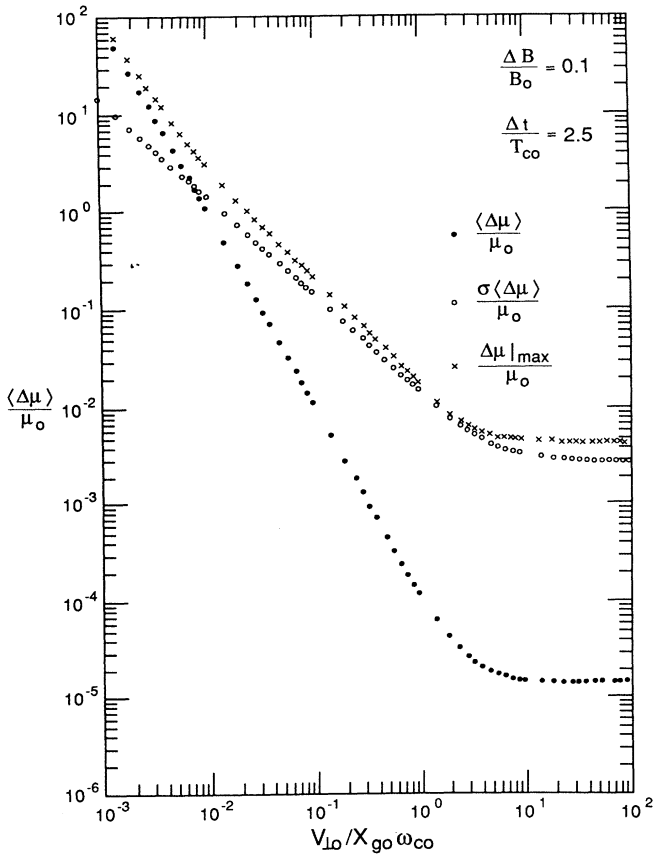

FIG. 8. For ensembles of 500 test particles, the quantities $\langle\Delta\mu\rangle/\mu_0$, $\sigma(\Delta\mu)/\mu_0$, and $\Delta\mu|_{max}/\mu_0$ are plotted as functions the initial particle velocity $v_{\perp 0}/x_{g0}\omega_{c0}$ for fixed values of $\Delta B/B_0$ and $\Delta t/\tau_{c0}$.

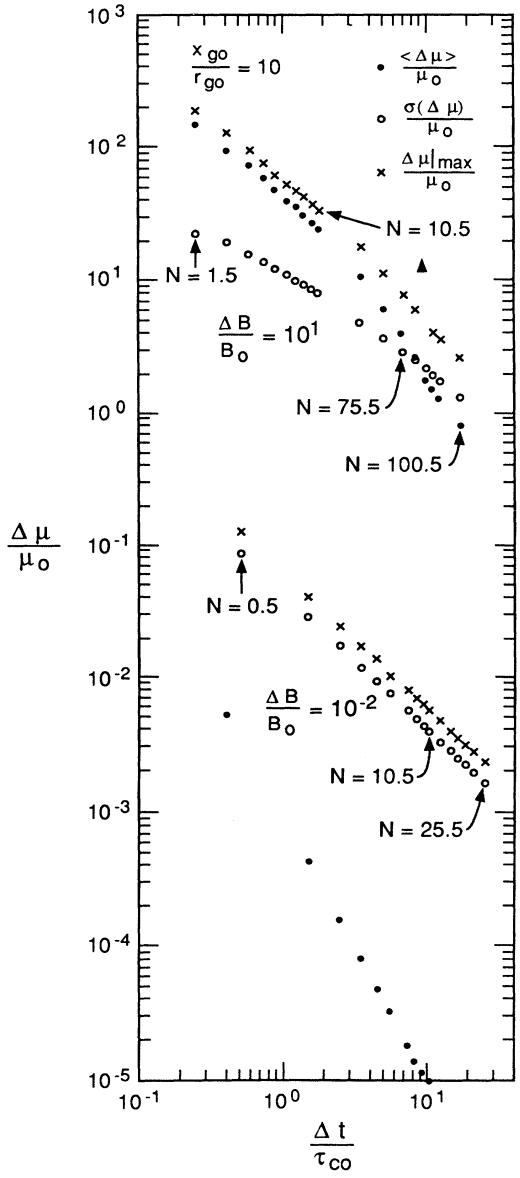

FIG. 9. For ensembles of 500 test particles, the quantities $\langle\Delta\mu\rangle/\mu_0$, $\sigma(\Delta\mu)/\mu_0$, and $\Delta\mu|_{max}/\mu_0$ are plotted as functions of $\Delta t/\tau_{c0}$ at the peaks in the $\Delta\mu$ vs Δt oscillations. The three sets of points in the upper portion of the graph are for $\Delta B/B_0 = 10^1$ and the three sets of points in the bottom portion of the graph are for $\Delta B/B_0 = 10^{-2}$.

and $x_{g0} \geq r_{g0}$. The validity of the expressions is not restricted to small values of $\langle \Delta\mu \rangle / \mu_0$ or to small values of $\sigma(\Delta\mu)/\mu_0$.

For $x_{g0} \ll r_{g0}$, the scaling relations are combined together to yield $\langle \Delta\mu \rangle \propto \Delta B^2 x_{g0}^0 v_{\perp 0}^2 \Delta t^{-2}$ and $\sigma(\Delta\mu) \propto |\Delta B|^1 x_{g0}^0 v_{\perp 0}^2 \Delta t^{-1}$. Dividing both relations by $\mu_0 = v_{\perp 0}^2 / B_0$, using $\tau_{c0} = 2\pi/\omega_{c0}$ and $r_{g0} = v_{\perp 0}/\omega_{c0}$, and introducing the constants C_3 and C_4 to replace the $\propto$ signs, these become

$$\langle \Delta\mu \rangle / \mu_0 = C_3 (\Delta B / B_0)^2 (\tau_{c0}/\Delta t)^2$$

and

$$\sigma(\Delta\mu)/\mu_0 = C_4 (|\Delta B|/B_0)^1 (\tau_{c0}/\Delta t)^1 .$$

Generating a new computer run at a maximum value of a $\Delta\mu$ versus Δt oscillation to obtain C_3 and C_4, the data are $\langle \Delta\mu \rangle / \mu_0 = 2.389 \times 10^{-6}$ and $\sigma(\Delta\mu)/\mu_0 = 8.107 \times 10^{-4}$ for $\Delta B / B_0 = 2.000 \times 10^{-2}$, $\Delta t / \tau_{c0} = 2.723$, and $x_{g0}/r_{g0} = 0.0$. These yield $C_3 \cong 4.43 \times 10^{-2}$ and $C_4 \cong 1.10 \times 10^{-1}$. Using these values yields, for $x_{g0} \ll r_{g0}$,

$$\frac{\langle \Delta\mu \rangle}{\mu_0} = 4.43 \times 10^{-2} \left[\frac{\Delta B}{B_0} \right]^2 \left[\frac{\tau_{c0}}{\Delta t} \right]^2 , \tag{17a}$$

$$\frac{\sigma(\Delta\mu)}{\mu_0} = 1.10 \times 10^{-1} \left[\frac{|\Delta B|}{B_0} \right]^1 \left[\frac{\tau_{c0}}{\Delta t} \right]^1 , \tag{17b}$$

which holds at the peaks of the $\Delta\mu$ versus Δt oscillations. Expressions (17) are valid for $\Delta t \geq 1.5\tau_{c0}$, $\Delta B \leq 10^{-1} B_0$, and $x_{g0} \ll r_{g0}$.

An important conclusion can be drawn at this point. For the case where Δt does not equal an integer number of gyroperiods, μ is found to be an adiabatic invariant. That is, $\Delta\mu \to 0$ as $\Delta t \to \infty$ (see Sec. I). The individual values of $\Delta\mu$ scale with Δt as does the standard deviation of the ensemble $\sigma(\Delta\mu)$, so by the definition given in Sec. I [see expression (3)], μ is an adiabatic invariant to first order in $\tau_{c0}/\Delta t$ when Δt is not equal to an exact integer multiple of τ_c.

Note that for $x_{g0} \geq r_{g0}$ [see expressions (16)],

$$\frac{\langle \Delta\mu \rangle}{\mu_0} \cong \frac{1}{2} \left[\frac{\sigma(\Delta\mu)}{\mu_0} \right]^2 , \tag{18}$$

and for $x_{g0} \ll r_{g0}$ [see expressions (16)],

$$\frac{\langle \Delta\mu \rangle}{\mu_0} \cong \frac{11}{3} \left[\frac{\sigma(\Delta\mu)}{\mu_0} \right]^2 . \tag{19}$$

Relations (18) and (19) will have strong consequences for the form of a Fokker-Planck equation that will describe the time evolution of a distribution function $f(\mu)$, as discussed in Ref. 22.

C. Measurements of $\Delta\mu$ at integer numbers of gyroperiods

As was seen in Fig. 4, the first adiabatic invariant μ is best conserved when the change in the magnetic induction occurs over an interval Δt that is exactly equal to an integer number of gyroperiods. The condition that Δt correspond to integer numbers of gyroperiods is given by expression (15). The minima in $\langle \Delta\mu \rangle$ and $\sigma(\Delta\mu)$ in Figs. 4 and 5 occur for Δt values satisfying this relation. Note, however, that the depths of these minima are not resolved in the two figures. Mathematically, Δt being equal to an integer number of gyroperiods corresponds to the action intergrals of the particle motion being completed [see expression (4)]. In the unbalanced-work picture of Sec. II, there is no unbalanced work when Δt is exactly equal to an integer number of gyroperiods, so $\Delta\mu = 0$ would be predicted in that picture. To attempt to understand the causes of the nonconservation of μ and to determine how $\langle \Delta\mu \rangle$ and $\sigma(\Delta\mu)$ scale with $\Delta B/B_0$, $\Delta t/\tau_{c0}$, and x_{g0}/r_{g0} when Δt is equal to an integer number of gyroperiods, test-particle computer simulations are run and the results are plotted in Figs. 10–13.

The $\Delta\mu$ values of the individual particles in two ensembles are shown in Fig. 10. Both sets of particles have undergone ramp magnetic-induction changes with Δt being exactly five gyroperiods long ($N = 5$). In one case (top panel) the particles had initial guiding centers located $4r_{g0}$ from the $x = 0$ plane, and in the other case (bottom panel) the particles' guiding center was located on the $x = 0$ plane. As can be seen in the figure, for $x_{g0}/r_{g0} = 4$ the $\Delta\mu$ values exhibit a sinusoidal dependence on the initial gyrophase angle θ_0 with one period per 2π of θ_0 and for $x_{g0}/r_{g0} = 0$ the $\Delta\mu$ values exhibit a sinusoidal depen-

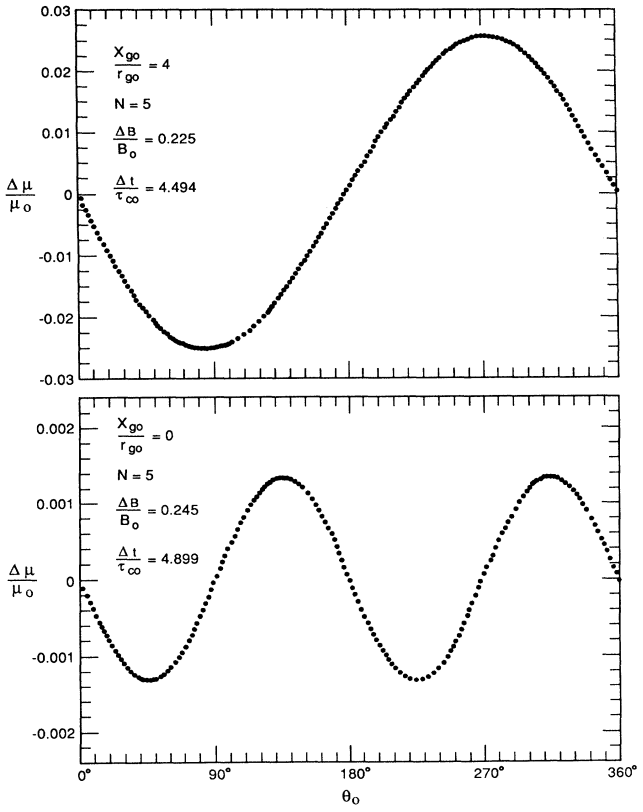

FIG. 10. For 360 test particles, $\Delta\mu/\mu_0$ is plotted as a function of θ_0 for Δt being exactly five gyroperiods. The top panel is for $x_{g0}/r_{g0} = 4$ and the bottom panel is for $x_{g0}/r_{g0} = 0$.

dence with two periods per 2π of θ_0. These are the same θ_0 periodicities that particles exhibited when Δt was unequal to exact numbers of gyroperiods (see, for example, Fig. 2), although the amplitude of the $\Delta\mu$ sinusoids is much smaller when Δt is exactly equal to integer numbers of gyroperiods.

In Fig. 11, $\langle\Delta\mu\rangle$ and $\sigma(\Delta\mu)$ are plotted as functions of $\Delta B/B_0$ at the first three minima of the $\Delta\mu$ versus Δt oscillation with x_{g0}/r_{g0} fixed. The three minima correspond to $N=1$, 2, and 3 in condition (15). In the right-hand panel it can be seen that the scaling of $\sigma(\Delta\mu)$ for each of the three minima is $\sigma(\Delta\mu)/\mu_0 \propto (\Delta B/B_0)^2$, with $\sigma(\Delta\mu)$ being larger when Δt is smaller (N is lower). In the left-hand panel it can be seen that $\langle\Delta\mu\rangle$ scales as $\langle\Delta\mu\rangle/\mu_0 \propto (|\Delta B|/B_0)^1$ for smaller values of $\Delta B/B_0$ and as $\langle\Delta\mu\rangle/\mu_0 \propto (|\Delta B|/B_0)^3$ at larger values of $\Delta B/B_0$. Thus, there appears to be one $\langle\Delta\mu\rangle$ scaling for weak perturbations and another $\langle\Delta\mu\rangle$ scaling for strong perturbations. Note that at smaller values of $\Delta B/B_0$ the $\langle\Delta\mu\rangle$ values are independent of Δt. The curves for the three Δt values coinciding, but at larger values of $\Delta B/B_0$ there is a Δt dependence to $\langle\Delta\mu\rangle$.

In Fig. 12 $\langle\Delta\mu\rangle$ and $\sigma(\Delta\mu)$ are plotted at minima in the $\Delta\mu$ versus Δt oscillations as functions of $\Delta t/\tau_{c0}$ for various values of $\Delta B/B_0$. The plots contain data for $N=1$, 2, 3, 4, 6, 8, 9, and 12, where N is the number of gyroperiods in Δt. As was the case in Fig. 9, the $\sigma(\Delta\mu)$ scaling is simpler than the $\langle\Delta\mu\rangle$ scaling. In the right-hand panel of Fig. 12 it can be seen that $\sigma(\Delta\mu)/\mu_0 \propto (\Delta t/\tau_{c0})^{-1}$ for each value of $\Delta B/B_0$. In the left-hand panel it is found that $\langle\Delta\mu\rangle/\mu_0 \propto (\Delta t/\tau_{c0})^0$ for the smaller values of $\Delta B/B_0$ and that $\langle\Delta\mu\rangle/\mu_0 \propto (\Delta t/\tau_{c0})^{-2}$ for the larger values of $\Delta B/B_0$. Again, there are different $\langle\Delta\mu\rangle$ scaling relations for weak and for strong perturbations.

In Fig. 13, $\sigma(\Delta\mu)$ and $\langle\Delta\mu\rangle$ are plotted as functions of the initial guiding-center position x_{g0}/r_{g0} at the first three minima of the $\Delta\mu$ versus Δt oscillation for two values of $\Delta B/\Delta t$. In the right-hand panel it is seen that $\sigma(\Delta\mu)$ scales as $\sigma(\Delta\mu)/\mu_0 \propto (x_{g0}/r_{g0})^0$ for $x_{g0} \ll r_{g0}$ and that it scales as $\sigma(\Delta\mu)/\mu_0 \propto (|x_{g0}|/r_{g0})^1$ for $x_{g0} \geq r_{g0}$. It is suspected that the breakpoint in these two scalings need not always occur at $x_{g0}=r_{g0}$. In the left-hand panel it is seen that $\langle\Delta\mu\rangle/\mu_0 \propto (x_{g0}/r_{g0})^0$ for $x_{g0} \ll r_{g0}$ and that $\langle\Delta\mu\rangle/\mu_0 \propto (x_{g0}/r_{g0})^2$ for x_{g0}/r_{g0} bigger than some critical value that depends on the size of $\Delta B/B_0$. Again, the scaling of $\langle\Delta\mu\rangle$ differs for weak and strong perturbations. Now the $\sigma(\Delta\mu)$ scaling is also found to exhibit this dichotomy.

For the limited parameter range that has been explored, the scalings of the $\Delta\mu$ quantities at complete gyroperiods (Figs. 11–13) can be summarized as follows.

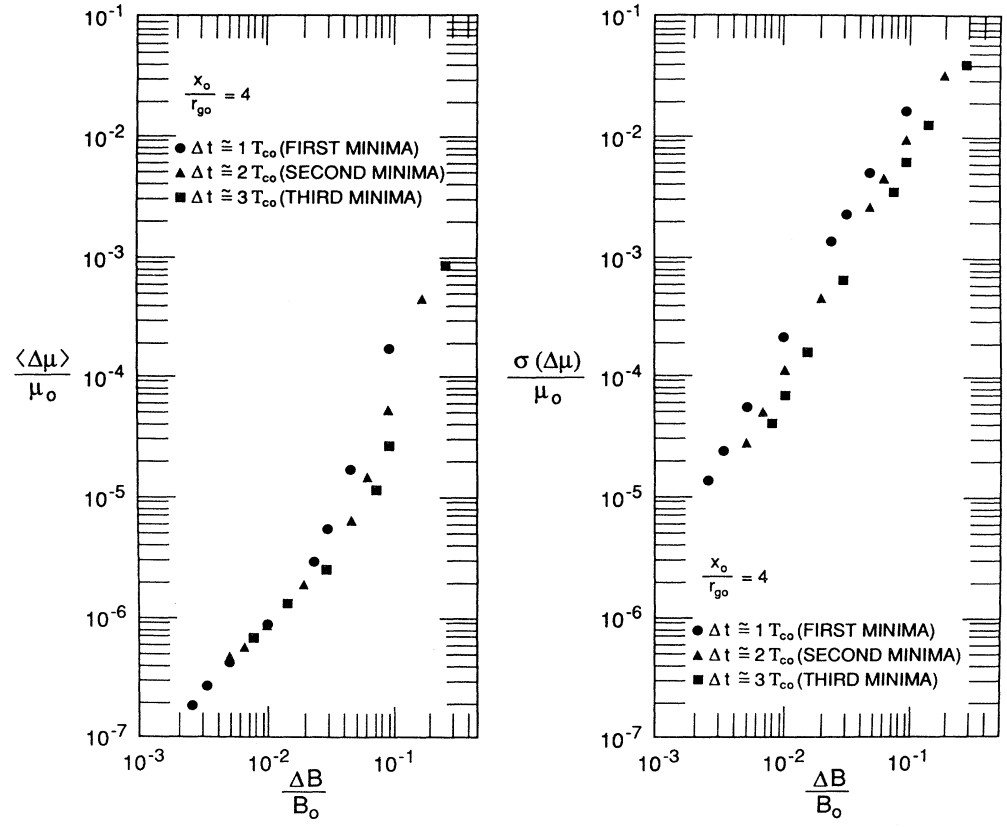

FIG. 11. For ensembles of 500–1500 particles, the statistical quantities $\langle\Delta\mu\rangle/\mu_0$ and $\sigma(\Delta\mu)/\mu_0$ are plotted as functions of $\Delta B/B_0$ at the first three minima of the $\Delta\mu$ vs Δt oscillations. The initial guiding-center position of the ensembles if fixed at $x_0/r_{g0}=4$.

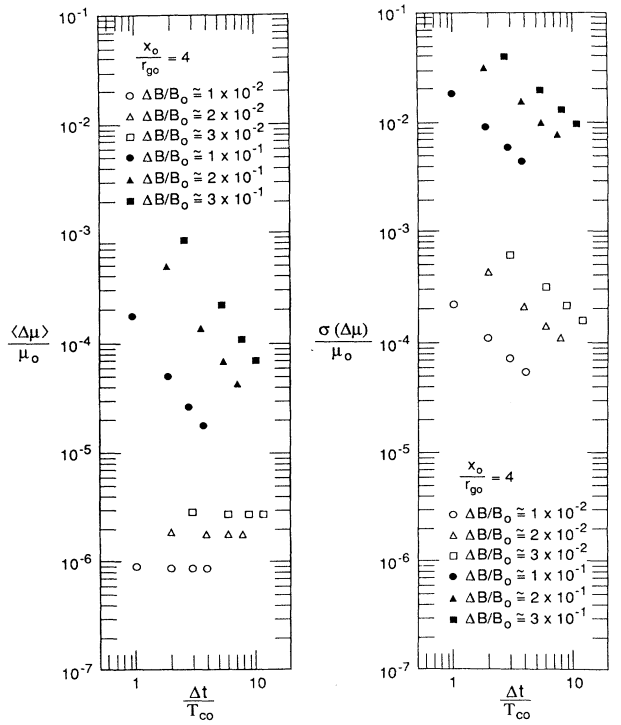

FIG. 12. For various values of $\Delta B/B_0$, the quantities $\langle \Delta\mu \rangle/\mu_0$ and $\sigma(\Delta\mu)/\mu_0$ are plotted as functions of $\Delta t/\tau_{c0}$ at minima in the $\Delta\mu$ vs Δt oscillation. Various values of $\Delta B/B_0$ are used and 500–1500 particles are used to make up the ensembles.

For $x_{g0} \gg r_{g0}$, the $\sigma(\Delta\mu)$ scaling is

$$\frac{\sigma(\Delta\mu)}{\mu_0} \propto \frac{|\Delta B|}{B_0} \left[\frac{|\Delta B|}{B_0} \frac{\tau_{c0}}{\Delta t} \frac{x_{g0}}{r_{g0}} \right]^1 \tag{20}$$

and for $x_{g0} \ll r_{g0}$ it is

$$\frac{\sigma(\Delta\mu)}{\mu_0} \propto \frac{|\Delta B|}{B_0} \left[\frac{|\Delta B|}{B_0} \frac{\tau_{c0}}{\Delta t} \right]^1 . \tag{21}$$

For $x_{g0} \ll r_{g0}$, the $\langle \Delta\mu \rangle$ scaling is

$$\frac{\langle \Delta\mu \rangle}{\mu_0} \propto \left[\frac{x_{g0}}{r_{g0}} \right]^0 \tag{22}$$

with unknown $\Delta B/B_0$ and $\Delta t/\tau_{c0}$ scalings. For $x_{g0} > r_{g0}$, the $\langle \Delta\mu \rangle$ scaling is dependent on the strength of the perturbation: it is

$$\frac{\langle \Delta\mu \rangle}{\mu_0} \propto \frac{|\Delta B|}{B_0} \left[\frac{|\Delta B|}{B_0} \frac{\tau_{c0}}{\Delta t} \frac{x_{g0}}{r_{g0}} \right]^0 \tag{23}$$

for smaller perturbations (smaller $\Delta B/\Delta t$ and x_{g0} values) and it is

$$\frac{\langle \Delta\mu \rangle}{\mu_0} \propto \frac{|\Delta B|}{B_0} \left[\frac{|\Delta B|}{B_0} \frac{\tau_{c0}}{\Delta t} \frac{x_{g0}}{r_{g0}} \right]^2 \tag{24}$$

for larger perturbations (larger $\Delta B/\Delta t$ and x_{g0} values).

The scaling relations (20)–(24) obtained for Δt being exactly equal to an integer number of gyroperiods differ fundamentally from the scaling relations (16) and (17) obtained for arbitrary Δt values. First, in the exact-integer scalings $\Delta B/B_0$ carries a different power than does $\tau_{c0}/\Delta t$. In the arbitrary-Δt scalings the powers of $\Delta B/B_0$ and $\tau_{c0}/\Delta t$ are the same. Second, in the exact-integer cases there are separate sets of scalings for strong perturbations and for weak perturbations. This dual scaling is not exhibited for arbitrary-Δt cases.

IV. THEORETICAL CALCULATIONS OF THE CHANGE IN μ FOR LINEAR RAMPS

In this section, it will be seen that a theoretical analysis of the orbits of charged particles provides information about the causes of the changes $\Delta\mu$ in the quantity μ when there is a time-changing magnetic induction. The analysis of the orbits will be found to validate and improve upon some of the quantitative results that were obtained by means of the computer simulations. As was explained in Sec. II, the work that the induction electric field does on a particle is responsible for the conservation of μ (see Sec. II). By performing more accurate analyses of this work, the small changes in μ can be calculated.

A. Work and the change in the first adiabatic invariant

For a change in the magnetic induction from B_0 to $B_0+\Delta B$, the change in the first adiabatic invariant $\Delta\mu=\mu-\mu_0$ is related to the work that the induction electric field does on the particle as it orbits in the time-changing magnetic induction. Denoting $\mu_0=\mu(t=0)$ and $\mu_{\text{final}}=\mu(t=\Delta t)$, where the change in the induction begins at time $t=0$ and ends at time $t=\Delta t$, the fractional change in μ is conveniently expressed as

$$\frac{\Delta\mu}{\mu_0} = \frac{\mu_{\text{final}}}{\mu_0} - 1 = \frac{v_{\perp\text{final}}^2}{v_{\perp 0}} \frac{B_0}{B_0 + (\Delta B/\Delta t)t} - 1 . \tag{25}$$

The perpendicular velocity $v_{\perp\text{final}}=v_\perp(t=\Delta t)$ is given by energy conservation to be $v_{\perp\text{final}}^2 = v_{\perp 0}^2 + (2/m)W$, where W is the work done on the particle. With this, relation (25) becomes

$$\frac{\Delta\mu}{\mu_0} = \frac{B_0}{B_0+\Delta B} \left[1 + \frac{2}{m v_{\perp 0}^2} W \right] - 1 , \tag{26}$$

which relates the fractional change in μ to the work W performed on the particle. Note that $W=W(\theta_0)$, and so $\Delta\mu/\mu$ will also be a function of the particle's initial gyrophase angle θ_0.

The work that the electric field performs on a particle is written $W=q\int \mathbf{E}\cdot d\mathbf{x}$, where $\int d\mathbf{x}$ is an integration over the path of the particle and q is the charge of the particle. For the time-dependent magnetic induction $\mathbf{B}=B(t)\hat{\mathbf{z}}$ described by Eqs. (7), the induction electric field is only in the y direction, so $W=q\int E_y dy$. Using expression (8) for E_y and writing $dy=v_y dt$, the work becomes

$$W=-\frac{q}{c}\frac{\Delta B}{\Delta t}\int_0^{\Delta t} x v_y dt \ , \tag{27}$$

where $x(t)$ and $v_y(t)$ can be obtained (in principle) by solving the orbit equations of the particle.

B. Circular-orbit approximation

A circular orbit that has constant gyrofrequency and that has no guiding-center drift is the simplest approximation that will yield some results for $\Delta\mu/\mu_0$. Consistent with the initial conditions (11), the circular orbit is described by

$$x \cong x_{g0}+\frac{v_{\perp 0}}{\omega_{c0}}\cos\left[\frac{q}{e}\omega_{c0}t+\theta_0\right] , \tag{28a}$$

$$v_y \cong -v_{\perp 0}\frac{q}{e}\cos\left[\frac{q}{e}\omega_{c0}t+\theta_0\right] , \tag{28b}$$

where θ_0 is the initial gyrophase angle of the particle. Expressions (28) describe circular gyromotion with no guiding-center drifts in a uniform, time-independent magnetic field. Inserting expressions (28) into relation (27) yields the work

$$W \cong \frac{e}{c}\frac{\Delta B}{\Delta t}v_{\perp 0}\frac{q}{e}\left[x_{g0}\int_0^t \cos\left[\frac{q}{e}\omega_{c0}t+\theta_0\right]dt + \frac{v_{\perp 0}}{\omega_{c0}}\int_0^t \cos^2\left[\frac{q}{e}\omega_{c0}t+\theta_0\right]dt\right] . \tag{29}$$

These integrals are straightforward with the use of $\sin(A)\cos(B)=\frac{1}{2}\sin(2A)$ and

$$\sin(C)-\sin(D)=2\cos[\tfrac{1}{2}(C+D)]\sin[\tfrac{1}{2}(C-d)] .$$

Inserting expression (29) into relation (27) yields

$$\frac{\Delta\mu}{\mu_0}=\frac{\Delta B}{B_0}\frac{\tau_{c0}}{\Delta t}\left[1+\frac{\Delta B}{B_0}\frac{t}{\Delta t}\right]^{-1} \times\left[\frac{2}{\pi}\frac{x_{g0}}{r_{g0}}\cos\left[\frac{q}{e}\frac{\omega_{c0}t}{2}+\theta_0\right]\sin\left[\frac{q}{e}\frac{\omega_{c0}t}{2}\right] + \frac{1}{2\pi}\cos\left[\frac{q}{e}\omega_{c0}t+2\theta_0\right]\sin\left[\frac{q}{e}\omega_{c0}t\right]\right] . \tag{30}$$

Note that for $t=$const, $\Delta\mu/\mu_0$ has a $\cos\theta_0$ dependence for $x_{g0}\gg r_{g0}$ and $\Delta\mu/\mu_0$ has a $\cos(2\theta_0)$ dependence for $x_{g0}\ll r_{g0}$, agreeing with the behavior of $\Delta\mu/\mu_0$ observed in Fig. 2.

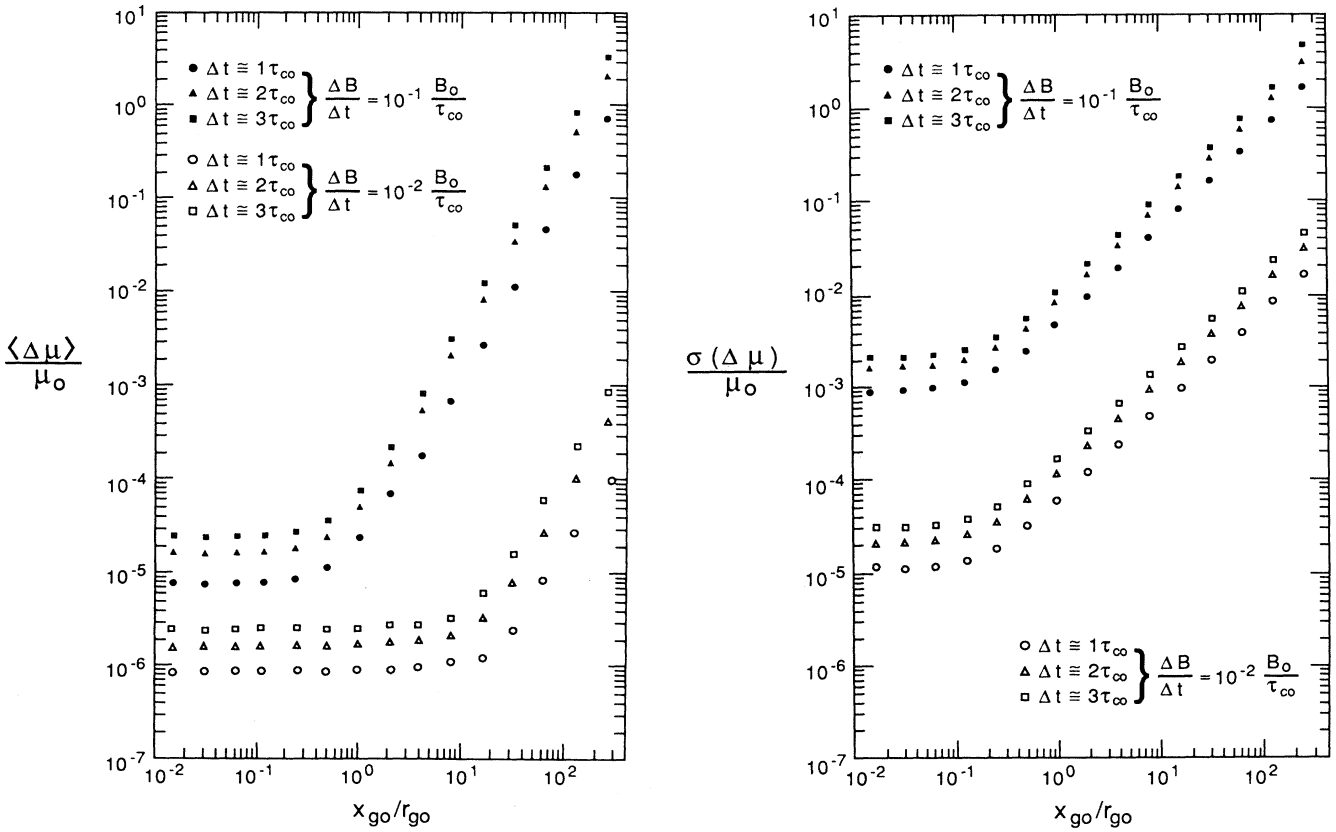

FIG. 13. The quantities $\langle\Delta\mu\rangle/\mu_0$ (left panel) and $\sigma(\Delta\mu)/\mu_0$ (right panel) are plotted as functions of the initial guiding-center position x_{g0}/r_{g0} at the first three minima in the $\Delta\mu$ vs Δt oscillation. Two values for $\Delta B/\Delta t$ are used.

As an aside, note that expression (30) predicts that $\Delta\mu \to 0$ as $\Delta t \to \infty$, which means that μ is an adiabatic invariant (to first order) in $\tau_{c0}/\Delta t$.

Taking the pitch-angle average $(1/2\pi)\int_0^{2\pi} d\theta_0$ of expression (30) yields

$$\left\langle \frac{\Delta\mu}{\mu_0} \right\rangle \cong 0 . \tag{31}$$

The standard deviation of the $\Delta\mu$ values is obtained by using the definition

$$\sigma(\Delta\mu)/\mu_0 = [\langle(\Delta\mu)^2\rangle - \langle\Delta\mu\rangle^2]^{1/2}/\mu_0 .$$

Taking the pitch-angle average of the square of expression (30) and inserting it and expression (31) into the above expression for $\sigma(\Delta\mu)/\mu_0$ and then taking $t=\Delta t$ yields

$$\frac{\sigma(\Delta\mu)}{\mu_0} \cong \frac{2^{1/2}}{\pi}\left[1+\frac{\Delta B}{B_0}\right]^{-1}\frac{\Delta B}{B_0}\frac{\tau_{c0}}{\Delta t} \times \left[\left(\frac{x_{g0}}{r_{g0}}\right)^2 \sin^2\left(\frac{\omega_{c0}\Delta t}{2}\right) + \tfrac{1}{16}\sin^2(\omega_{c0}\Delta t)\right]^{1/2} . \tag{32}$$

This expression captures a behavior seen in the test-particle simulations of Sec. III: For $x_{g0} \gg r_{g0}$ the periodicity of $\sigma(\Delta\mu)$ goes as $|\sin(\frac{1}{2}\omega_{c0}\Delta t)|$, and as $x_{g0} \to 0$ the periodicity goes to $|\sin(\omega_{c0}\Delta t)|$. Provided that Δt is not exactly equal to an integer number gyroperiods, expression (32) is a very good fit to the test-particle-simulation data in both the $x_{g0} \gg r_{g0}$ regime and the $x_{g0} \to 0$ regime. For $x_{g0} \gg r_{g0}$, the theoretical expression (32) differs from the computer-simulation fits given by expression (16a) by 5.0% for $\Delta B \ll B_0$, and for $x_{g0} \ll r_{g0}$ expression (32) differs from the simulation fits given by expression (17a) by 1.8%. Hence, there is good agreement between the computer-simulation results and the analytic calculations. In the limits of $x_{g0}/r_{g0} \ll 1$ and $x_{g0}/r_{g0} \gg 1$, $\Delta\mu/\mu_0$ can be maximized with respect to θ_0 to yield

$$\left[\frac{\Delta\mu}{\mu_0}\right]_{\max} \cong \frac{2}{\pi}\frac{\Delta B}{B_0}\frac{\tau_{c0}}{\Delta t}\frac{x_{g0}}{r_{g0}} \times \left[1+\frac{\Delta B}{B_0}\right]^{-1}\left|\sin\left(\frac{\omega_{c0}\Delta t}{2}\right)\right| \quad \text{for } x_{g0} \gg r_{g0} , \tag{33a}$$

$$\left[\frac{\Delta\mu}{\mu_0}\right]_{\max} \cong \frac{\Delta B}{B_0}\frac{\tau_{c0}}{\Delta t}\left[1+\frac{\Delta B}{B_0}\right]^{-1}|\sin(\omega_{c0}\Delta t)| \quad \text{for } x_{g0} \ll r_{g0} . \tag{33b}$$

A very simple derivation of the conservation of μ often used in textbooks (for example, Refs. 23–27) is to use a circle to approximate the orbit and to calculate the work done on the particle over exactly one full period of the orbit. Expression (30) for $\Delta\mu/\mu_0$ agrees with these derivations at the close of a circular orbit: $\Delta\mu/\mu_0 = 0$ when $t=\Delta t=\tau_{c0}=2\pi/\omega_{c0}$. However, expression (30) goes beyond the textbook derivations since it includes cases where the gyro-orbits are not closed during the time when the magnetic induction changes. Expression (30) quantifies the unbalanced-work picture of Sec. II. The fact that expression (30) agrees with the computer simulations confirms that the major part of the $\Delta\mu/\mu_0$ comes from the unbalanced work around the gyro-orbit.

Note that the circular-orbit approximation did not obtain the correct values for $\langle\Delta\mu\rangle/\mu_0$, which were found in the simulations to be nonzero but small (see Sec. III B), nor does the circular-orbit approximation obtain the correct values for $\Delta\mu/\mu_0$ when Δt is equal to an integral number of gyroperiods, which were also found to be nonzero but small (see Sec. III C).

C. Limit of $\Delta t \to 0$

When the magnetic-induction change is very rapid, charged particles are impulsively accelerated by a strong-induction electric field during the brief change. For magnetic-induction changes occurring over such brief time intervals, a circular orbit is a very poor approximation to the true orbit, and so the expressions for $\Delta\mu$ obtained in Sec. IV B should fail to describe $\Delta\mu$ when Δt is very small. The circular (unperturbed) orbit requires $|\mathbf{E}| \ll (1/c)|\mathbf{v}\times\mathbf{B}|$, since electric-field accelerations were ignored. Using expression (8) for $\mathbf{E}$, the ratio of electric-field to magnetic-field accelerations during the change in B is $|\mathbf{E}|/[(1/c)|\mathbf{v}\times\mathbf{B}|] = (\Delta B/B_0)(x/v_\perp)(1/\Delta t)$. Hence, no matter how small ΔB and x are, this ratio becomes infinite as $\Delta t \to 0$. Accordingly, the electric-field force in the particle's equation of motion cannot be ignored when calculating $\Delta\mu/\mu_0$ as $\Delta t \to 0$, but the magnetic-field force can be. In fact, for $\Delta t/\tau_{c0} \ll \frac{1}{4}$, the $\mathbf{v}\times\mathbf{B}$ force has very little effect on the orbit, and it can therefore be ignored. For the electromagnetic-field geometry given by expressions (7) and (8), the work done on a particle is given by $W = q\int E_y dy$, where $E_y(x)$ is evaluated along the particle's orbit. If the change in the magnetic induction is rapid enough, then the particle will not move appreciably in the x direction while the work is being done, and so E_y will be approximately constant during the work. This requirement can be written $\Delta E_y/E_y \ll 1$, which, with the use of Eq. (8), can be written $\Delta x/x_0 = v_x\Delta t/x_0 \ll 1$. The maximum value of v_x is $v_{\perp 0}$; with this and with $r_{g0} = v_{\perp 0}\tau_{c0}/2\pi$, the requirement becomes $\Delta t/\tau_{c0} \ll (1/2\pi)(x_0/r_{g0})$. If this condition is met, then E_y is approximately constant and it can be pulled through the integration in $q\int E_y dy$, and the work expression becomes $W = qE_y\Delta y$, where Δy is the distance that the particle moves in the y direction during the impulsive acceleration. If $\Delta t/\tau_{c0} \ll \frac{1}{4}$ is met, then rectilinear motion can be used to calculate Δy which yields the expression $\Delta y = v_{y0}\Delta t + (q/2m)E_y\Delta t^2$. Inserting this expression into $W = qE_y\Delta y$ and using Eq. (8) for E_y yields

$$W = -(q/c)\Delta B v_{y0}x_0 + (q^2/2mc^2)\Delta B^2 x_0^2 ,$$

where x_0 is the initial position of the particle. Using ini-

tial conditions (11a) and (11d) for particles with the same initial guiding center and same initial perpendicular velocity, the expression for the work done by the induction electric field on a positive particle becomes

$$W=m\omega_{c0}^2\frac{\Delta B}{B_0}\left[\frac{1}{2}\frac{\Delta B}{B_0}x_{g0}^2+r_{g0}x_{g0}\left[1+\frac{\Delta B}{B_0}\right]\cos\theta_0 + r_{g0}^2\left[1+\frac{1}{2}\frac{\Delta B}{B_0}\right]\cos^2\theta_0\right], \quad (34)$$

where θ_0 is the initial gyrophase angle of a particle and where $v_{\perp 0}=r_{g0}\omega_{c0}$ was used. Inserting this into expression (26) yields, at $t=\Delta t$,

$$\frac{\Delta\mu}{\mu_0}=\frac{\Delta B/B_0}{1+\Delta B/B_0}\left[\left[\frac{\Delta B}{B_0}\frac{x_{g0}^2}{r_{g0}^2}-1\right] +2\frac{x_{g0}}{r_{g0}}\left[1+\frac{\Delta B}{B_0}\right]\cos\theta_0 +2\left[1+\frac{1}{2}\frac{\Delta B}{B_0}\right]\cos^2\theta_0\right]. \quad (35)$$

Note that this expression is not limited to $\Delta B/B_0$ small.

The gyrophase-angle average $(1/2\pi)\int_0^{2\pi}d\theta_0$ of expression (35) yields

$$\frac{\langle\Delta\mu\rangle}{\mu_0}=\frac{1}{1+(\Delta B/B_0)}\left[\frac{\Delta B}{B_0}\right]^2\left[\frac{x_{g0}^2}{r_{g0}^2}+\frac{1}{2}\right]. \quad (36)$$

In Ref. 28 a similar expression was derived for particles moving in a cylindrically symmetric induction electric field $E_\theta=(1/2c)(\Delta B/\Delta t)r$; expression (36) (which is valid for an electric field that is antisymmetric about a plane rather than a line) is equivalent to expression (8) of Ref. 28 in the limit of $x_{g0}\gg r_{g0}$ and when the induction electric field is reduced by a factor of $\frac{1}{2}$. Taking the root-mean-square gyrophase average of expression (35) and inserting it and expression (36) into

$$\sigma(\Delta\mu)/\mu_0=[\langle(\Delta\mu)^2\rangle-\langle\Delta\mu\rangle^2]^{1/2}\mu_0$$

yields

$$\frac{\sigma(\Delta\mu)}{\mu_0}=\frac{1}{1+\Delta B/B_0}\frac{\Delta B}{B_0}\left[2\left[\frac{x_0}{r_{g0}}\right]^2\left[1+\frac{\Delta B}{B_0}\right]^2+\frac{1}{2}\left[1+\frac{1}{2}\frac{\Delta B}{B_0}\right]^2\right]^{1/2}. \quad (37)$$

Inspecting relation (35), the value of $\Delta\mu/\mu_0$ is found to be maximum for an initial gyrophase angle $\theta_0=0°$, yielding

$$\frac{\Delta\mu|_{\max}}{\mu_0}=\frac{\Delta B}{B_0}\left[1+2\frac{x_{g0}}{r_{g0}}+\frac{x_{g0}^2}{r_{g0}^2}\frac{\Delta B/B_0}{1+\Delta B/B_0}\right]. \quad (38)$$

Where tested, the values of $\langle\Delta\mu\rangle/\mu_0$, $\sigma(\Delta\mu)/\mu_0$, and $\Delta\mu|_{\max}/\mu_0$ are identical to the values obtained from the test-particle simulations, hence the agreement between the theory and the computer data is excellent. Note that relation (18) holds for expressions (36) and (37) in the limit of $x_{g0}\gg r_{g0}$ for all values of $\Delta B/B_0$.

D. Exact orbits from the pumped harmonic-oscillator equation

It is desirable to obtain exact analytic solutions to the orbit equations for a charged particle in the time-varying magnetic induction. With the magnetic induction $B_z(t)$ given by expression (7) and the electric field given by expression (8), the equations of motion (10) are combined to yield

$$\frac{\partial}{\partial t}\left[\frac{1}{\omega_c}\frac{\partial^2 x}{\partial t^2}\right]=-\omega_c\frac{\partial x}{\partial t}-\omega_{c0}\frac{\Delta B}{B_0}\frac{1}{\Delta t}x, \quad (39)$$

where $\omega_c=eB/mc$, with $B=B(t)$, and where $\omega_{c0}=eB_0/mc$. Since $B=B_0+(\Delta B/\Delta t)t$ [see Eq. (7)], $\partial\omega_c/\partial t=(\omega_{c0}/B_0)(\Delta B/\Delta t)$. Thus, the right-hand side of this relation becomes $-(\partial/\partial t)(\omega_c x)$. Integrating $\int_0^t dt$ with the initial values for x and $\partial^2x/\partial t^2$, and noting that there is no electric field term in $(\partial^2x/\partial t^2)_{t=0}$, the pumped harmonic-oscillator equation

$$\frac{\partial^2 x}{\partial t^2}+\omega_c^2 x=\omega_{c0}\omega_c x_{g0} \quad (40)$$

is obtained. For $x_{g0}=0$, Eq. (40) reduces to the unpumped harmonic-oscillator equation that was considered by Kulsrud.[14] Changing variables from t to $\tau\equiv(\omega_{c0}/\epsilon)^{1/2}(1+\epsilon t)$, where $\epsilon=\Delta B/(B_0\Delta t)$, the pumped harmonic-oscillator equation becomes

$$(\partial^2x/\partial\tau^2)+\tau^2x=(\omega_{c0}/\epsilon)^{1/2}x_{g0}\tau.$$

The homogeneous equation obtained by setting the right-hand side of this expression to zero is a Lommel transformation of Bessel's equation.[29] According to expression 9.1.51 of Ref. 30 and the above definition of τ, this homogeneous equation has a solution

$$x_h(t)=\left[\frac{\omega_{c0}}{\epsilon}\right]^{1/4}(1+\epsilon t)^{1/2}\times\left[\alpha_1\mathcal{C}_{1/4}^{(1)}\left[\frac{1}{2}\frac{\omega_{c0}}{\epsilon}(1+\epsilon t)^2\right] +\alpha_2\mathcal{C}_{1/4}^{(2)}\left[\frac{1}{2}\frac{\omega_{c0}}{\epsilon}(1+\epsilon t)^2\right]\right], \quad (41)$$

where $\mathcal{C}^{(1)}$ and $\mathcal{C}^{(2)}$ are either the pair of Bessel functions J and Y or the pair of Hankel functions $H^{(1)}$ and $H^{(2)}$. If $x_{g0}=0$, then the exact orbit is given by expression (41) and α_1 and α_2 are obtained from initial conditions (11a) and (11c).

A particular solution to the inhomogeneous differential equation (40) can be obtained by using the method of variation of parameters. Taking $\mathcal{C}_{1/4}^{(1)}=H_{1/4}^{(1)}$ and $\mathcal{C}_{1/4}^{(2)}=H_{1/4}^{(2)}$, the needed Wronskian is found with the use of expression 9.1.17 of Abramowitz and Stegun[30] to be

$$W\{\tau^{1/2}H_{1/4}^{(1)}(\tfrac{1}{2}\tau^2),\tau^{1/2}H_{1/4}^{(2)}(\tfrac{1}{2}\tau^2)\}=-8i/\pi.$$

Defining $\psi=\tau^2/2$, the particular solution is written

$$x_p(t)=\frac{i\pi}{8}\frac{\omega_{c0}x_{g0}}{\epsilon}\left[\frac{2\epsilon}{\omega_{c0}}\right]^{1/4}(1+\epsilon t)^{1/2}\left[-H^{(1)}_{1/4}\left[\frac{\omega_{c0}}{2\epsilon}(1+\epsilon t)^2\right]\int^{\omega_{c0}/[2\epsilon(1+\epsilon t)^2]}\psi^{1/4}H^{(2)}_{1/4}(\psi)d\psi\right.$$
$$\left.+H^{(2)}_{1/4}\left[\frac{\omega_{c0}}{2\epsilon}(1+\epsilon t)^2\right]\int^{\omega_{c0}/[2\epsilon(1+\epsilon t)^2]}\psi^{1/4}H^{(1)}_{1/4}(\psi)d\psi\right] . \quad (42)$$

It is unlikely that the integrals in expression (42) can be performed analytically, even if asymptotic expansions for the $H_{1/4}$ functions are made and the series are integrated term by term. Thus, the use of this exact expression is limited.

V. MAGNETIC-INDUCTION RAMPS WITH DIFFERING FUNCTIONAL FORMS

In this section, the breaking of the first adiabatic invariant μ by linear-ramp magnetic-induction variations is compared with the breaking of the invariant by two other forms of ramps. One form is a hyperbolic tangent and the other is one-half period of a sine wave. The three ramps are displayed in the top panel of Fig. 14. Within the three ramps the time variation of the magnetic induction is

$$B=B_0+\frac{\Delta B}{2}\left[1+\frac{t}{\Delta t/2}\right] \quad \text{for } -\frac{\Delta t}{2}\le t\le\frac{\Delta t}{2} \quad (43)$$

for the linear ramp,

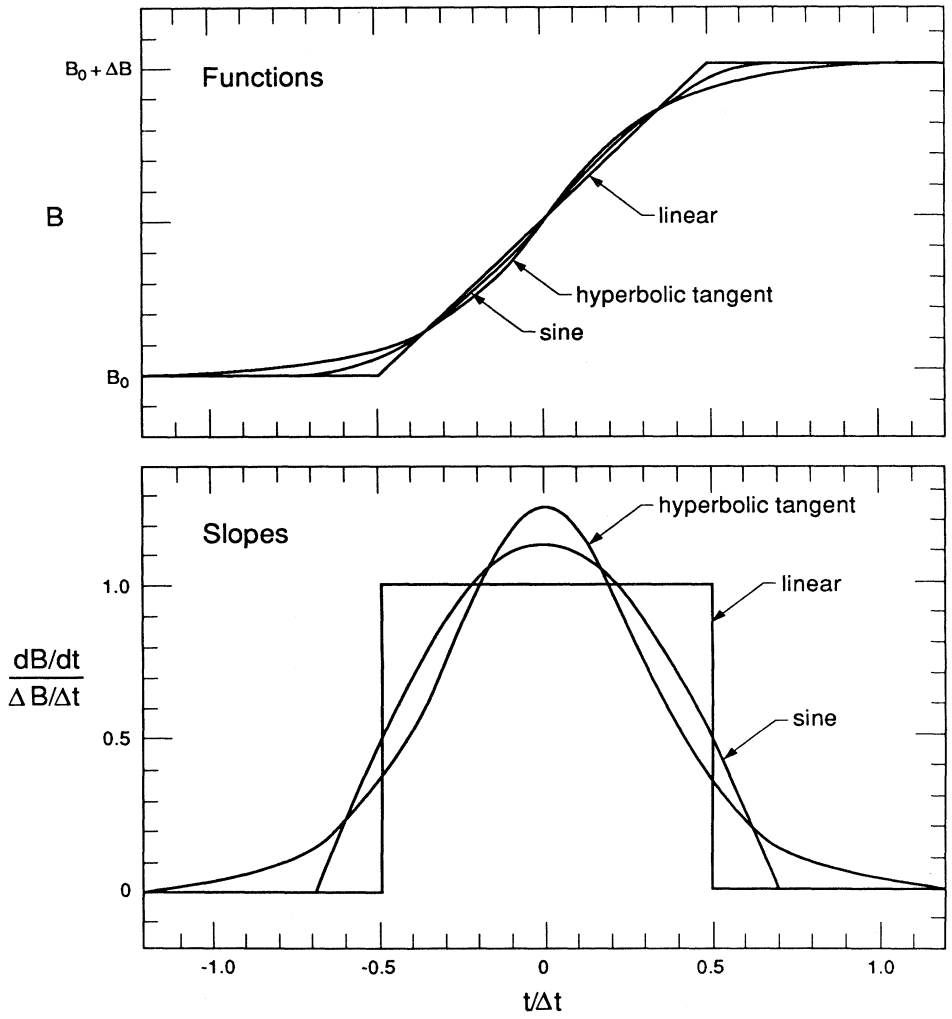

FIG. 14. In the top panel three different ramp functions $B(t)$ are compared, and in the bottom panel their time derivatives are compared.

$$B = B_0 + \frac{\Delta B}{2}\left[1+\sin\left[2.258\frac{t}{\Delta t}\right]\right] \quad \text{for } -0.696\Delta t \le t \le 0.696\Delta t \tag{44}$$

for the sine-wave ramp, and

$$B = B_0 + \frac{\Delta B}{2}\left[1+\tanh\left[2.507\frac{t}{\Delta t}\right]\right] \quad \text{for } -\infty \le t \le \infty \tag{45}$$

for the hyperbolic-tangent ramp. For the linear ramp before $t=-\Delta t/2$ and for the sine-wave ramp before $t=-0.696\Delta t$, the induction is constant at $B=B_0$ and after time $t=\Delta t/2$ and $t=0.696\Delta t$, respectively, the linear ramp and sine-wave ramp have $B=B_0+\Delta B$. For all three ramps, the jump in magnetic induction is ΔB. With the width of the linear ramp taken to be Δt, the widths of the other two ramps are determined by minimizing the integral from $t=-\infty$ to $t=+\infty$ of the square of the difference between the first derivatives of the ramps compared with the first derivative of the linear ramp. This is a least-squares fit of the first derivatives. This minimization process yields the numerical factors of 2.257 979 and 2.5074 in Eqs. (44) and (45). The first derivatives of the ramps are plotted in the bottom panel of Fig. 14. In addition to the mean-squared deviation of the sine and hyperbolic-tangent curves from the linear curve being minimized, the areas under the curves are equal.

Some expected $\Delta\mu$ values for the three ramps are as follows. According to Kulsrud's analysis[14] of the unpumped harmonic-oscillator equation[see Eq. (40)] $(\partial^2 x/\partial t^2)+\omega_c^2 x=0$ (which applies only to particles with $x_{g0}=0$), the functional form of the $\Delta\mu$ versus Δt relation in the adiabatic limit is governed by the number of continuous derivatives that there are in the ramp function. Kulsrud's analysis predicts $\sigma(\Delta\mu)/\mu_0 \approx Z_{N+1}/(2\omega_{c0})^{N+2}$ and $\langle\Delta\mu\rangle/\mu_0=0$, where N is the number of continuous derivatives in the ramp and where Z_{N+1} is the jump in the $(N+1)$st derivative of ω_c at the discontinuity. These yield

$$\frac{\sigma(\Delta\mu)}{\mu_0} \propto \left[\frac{\Delta B}{B_0}\right]^1\left[\frac{\tau_{c0}}{\Delta t}\right]^{N+1}, \tag{46a}$$

$$\frac{\langle\Delta\mu\rangle}{\mu_0}=0 . \tag{46b}$$

The linear ramp has 0 continuous derivatives, the sine-wave ramp has one continuous derivative, and the hyperbolic-tangent ramp has an infinite number of continuous derivatives. For $\Delta B/B_0$ small, as $\Delta t/\tau_{c0}\to\infty$ (the adiabatic limit) the expected $\Delta\mu$ values for the hyperbolic-tangent ramp go as[28,31,32] $\Delta\mu \propto e^{-\Delta t}$. Besides checking these ramps in the asymptotic limits $(\Delta t/\tau_{c0}\to\infty)$, the computer simulations will be used to examine the behavior of μ for all values of Δt.

For ensembles of particle that have experienced changes in the magnetic induction that take the forms of the linear ramp, the sine-wave ramp, and the hyperbolic-tangent ramp, the mean and standard deviation of $\Delta\mu$ are compared in Fig. 15. The particles in the ensembles all have the same initial value of μ and the same initial guiding-center position, and the averages are over the initial gyrophase angle θ_0. For $\Delta t/\tau_{c0}\to 0$, it is seen that the three types of ramps produced identical values of $\Delta\mu/\mu_0$ and that for $\Delta t/\tau_{c0}\le 0.5$ the three ramps produce very similar $\Delta\mu/\mu_0$ values. For $\Delta t/\tau_{c0}>0.5$ the $\Delta\mu/\mu_0$ values are very different. A check on the peaks in the oscillations shows that $\langle\Delta\mu\rangle/\mu_0 \propto (\Delta t/\tau_{c0})^{-2}$ and $\sigma(\Delta\mu)/\mu_0 \propto (\Delta t/\tau_{c0})^{-1}$ for the linear ramp (as found in Secs. III and IV) and that $\langle\Delta\mu\rangle/\mu_0 \propto (\Delta t/\tau_{c0})^{-4}$ and $\sigma(\Delta\mu)/\mu_0 \propto (\Delta t/\tau_{c0})^{-2}$ for the sine-wave ramp. The $\sigma(\Delta\mu)/\mu_0$ scalings agree with the predictions of Kulsrud[14] [see Eq. (46a)], since the linear ramp has 0 continuous derivatives and the sine-wave ramp has one continuous derivative. For the linear ramp, Kulsrud's $x_{g0}=0$ analysis predicts that

$$\sigma(\Delta\mu)/\mu_0 = 1/(8\pi)(\Delta B/B_0)^1(\tau_{c0}/\Delta t)^1 ,$$

whereas the theory of Sec. IV B (which agrees with the computer simulations) for $x_{g0}=0$ obtains

$$\sigma(\Delta\mu)/\mu_0 = 2^{1/2}/(4\pi)(\Delta B/B_0)^1(\tau_{c0}/\Delta t)^1$$

[see expression (32)] at the peaks in the $\Delta\mu$ versus Δt oscillations. Note also that Kulsrud's analysis predicts $\langle\Delta\mu\rangle=0$ for all ramps, whereas $\langle\Delta\mu\rangle\neq 0$ for the ramps (see Fig. 15). For the hyperbolic-tangent ramp, the values of Fig. 15 yield $\langle\Delta\mu\rangle/\mu_0 \propto e^{-7.3(\Delta t/\tau_{c0})}$ and $\sigma(\Delta\mu/\mu_0 \propto e^{-3.8(\Delta t/\tau_{c0})}$ for larger $\Delta t/\tau_{c0}$ values. These scalings agree fairly well with the predictions of Hertweck and Schluter[28] that $\langle\Delta\mu\rangle/\mu_0 \propto e^{-7.9(\Delta t/\tau_{c0})}$ for the hyperbolic-tangent ramp of expression (45).

Note in Fig. 7 that the periodicity with Δt of the oscillation in the sine-ramp curves differs from the periodicity with Δt of the linear-ramp curves, with the period of the sine curves being $\sim 0.7\tau_{c0}$. The length of the sine ramp is $2(0.696)\Delta t = 1.39\Delta t$ [see expression (44)]. Thus, when Δt increases by $0.7\tau_{c0}$, the length of the ramp increases by $0.97\tau_{c0}$. Hence, the periodicity of the sine-ramp curves agrees with the periodicity that is described by the unbalanced-work picture of Sec. II, as does the periodicity of the linear-ramp curves.

Note in Fig. 15 that there is no oscillation of $\langle\Delta\mu\rangle$ or $\sigma(\Delta\mu)$ versus Δt for the hyperbolic-tangent ramp. This is also the case for single particles; a particle that starts at the same gyrophase angle θ_0 at the same time $t=-t_0$, where $t_0 \gg \Delta t$, has no oscillation of $\Delta\mu$ versus Δt. However, individual particles have $\Delta\mu$ versus t oscillations during the hyperbolic-tangent-ramp magnetic-induction change, as can be seen in Fig. 16. Here, $\Delta\mu/\mu_0$ is plotted as a function of time for two particles, one (top panel) experiencing a ramp with $\Delta t = 2\tau_{c0}$ and the other (bottom panel) experiences a quicker ramp with $\Delta t = 0.5\tau_{c0}$. In both cases, the $\Delta\mu$ values increase as $\Delta\mu \propto e^{c_1 t + i\omega_c t}$, where the value of c_1 depends on the ramp height ΔB and

the ramp width Δt. Note for the top panel that $\Delta\mu(t=0) \gg \Delta\mu(t \to +\infty)$. In fact, the values of $\sigma(\Delta\mu)$ and $\langle \Delta\mu \rangle$ at time $t=0$ (center of the ramp) are similar to the $\sigma(\Delta\mu)$ and $\langle \Delta\mu \rangle$ values obtained for the linear ramp (see Fig. 15 at $\Delta t/\tau_{c0} \approx 2$); however, the $\Delta\mu$ values in the hyperbolic-tangent ramp decrease with time after the ramp center. Note in Fig. 16 that the rate of exponential falloff for $t>0$ is slower than the rate of exponential gain for $t<0$.

The Δt scalings of $\sigma(\Delta\mu)$ and $\langle \Delta\mu \rangle$ were obtained from Fig. 15. Two new figures will be generated to determine the ΔB and x_{g0} scalings. For ensembles of particles that have experienced hyperbolic-tangent ramps, the final values of $\sigma(\Delta\mu)$ and $\langle \Delta\mu \rangle$ are plotted as functions of the ramp height ΔB in Fig. 17. In the left-hand panel the magnetic induction decreases in the ramps ($\Delta B<0$), and in the right-hand panel the induction increases in the ramps ($\Delta B>0$). Here, for $|\Delta B/B_0| \ll 1$, the scalings $\langle \Delta\mu \rangle/\mu_0 \propto (\Delta B/B_0)^2$ and $\sigma(\Delta\mu)/\mu_0 \propto (|\Delta B|/B_0)^1$ are clearly seen. Note the curious behavior in the right-hand panel that for $\Delta B/B_0 \gg 1$ a maximum value of $\Delta\mu/\mu_0$ is reached. This is very different from the behavior of particles in linear ramps (Fig. 6), where $\Delta\mu$ increased indefinitely as ΔB increased. The $\sigma(\Delta\mu)$ and $\langle \Delta\mu \rangle$ values for ensembles of particles experiencing hyperbolic-tangent ramps are plotted as functions of x_{g0}/r_{g0} in Fig. 18. As can be seen, there are two regions for the scalings: $x_{g0}/r_{g0} \ll 1$ and $x_{g0}/r_{g0} > 1$. For $x_{g0}/r_{g0} \ll 1$, the values of $\langle \Delta\mu \rangle/\mu_0$ and $\sigma(\Delta\mu)/\mu_0$ reach a constant value. This behavior is very similar to that observed with linear ramps (see Fig. 7). For $x_{g0}/r_{g0} \ll 1$, the scalings $\langle \Delta\mu \rangle/\mu_0 \propto (x_{g0}/r_{g0})^0$ and $\sigma(\Delta\mu)/\mu_0 \propto (x_{g0}/r_{g0})^0$ are obtained from Fig. 18. For $x_{g0}/r_{g0} > 1$, the scalings $\langle \Delta\mu \rangle/\mu_0 \propto (x_{g0}/r_{g0})^2$ and $\sigma(\Delta\mu)/\mu_0 \propto (|x_{g0}|/r_{g0})^1$ are obtained. Putting these scalings together and using one $\sigma(\Delta\mu)$ and one $\langle \Delta\mu \rangle$ data point from Fig. 15 yields the fits to the test-particle computer-simulation data

$$\frac{\langle \Delta\mu \rangle}{\mu_0} \approx 34.3 \left[\frac{\Delta B}{B_0} \right]^2 \left[\frac{x_{g0}}{r_{g0}} \right]^2 e^{-7.3\Delta t/\tau_{c0}}, \tag{47a}$$

$$\frac{\sigma(\Delta\mu)}{\mu_0} \approx 13.4 \left[\frac{|\Delta B|}{B_0} \right]^1 \left[\frac{|x_{g0}|}{r_{g0}} \right]^0 e^{-3.8\Delta t/\tau_{c0}} \tag{47b}$$

for $x_{g0}/r_{g0} > 1$ and

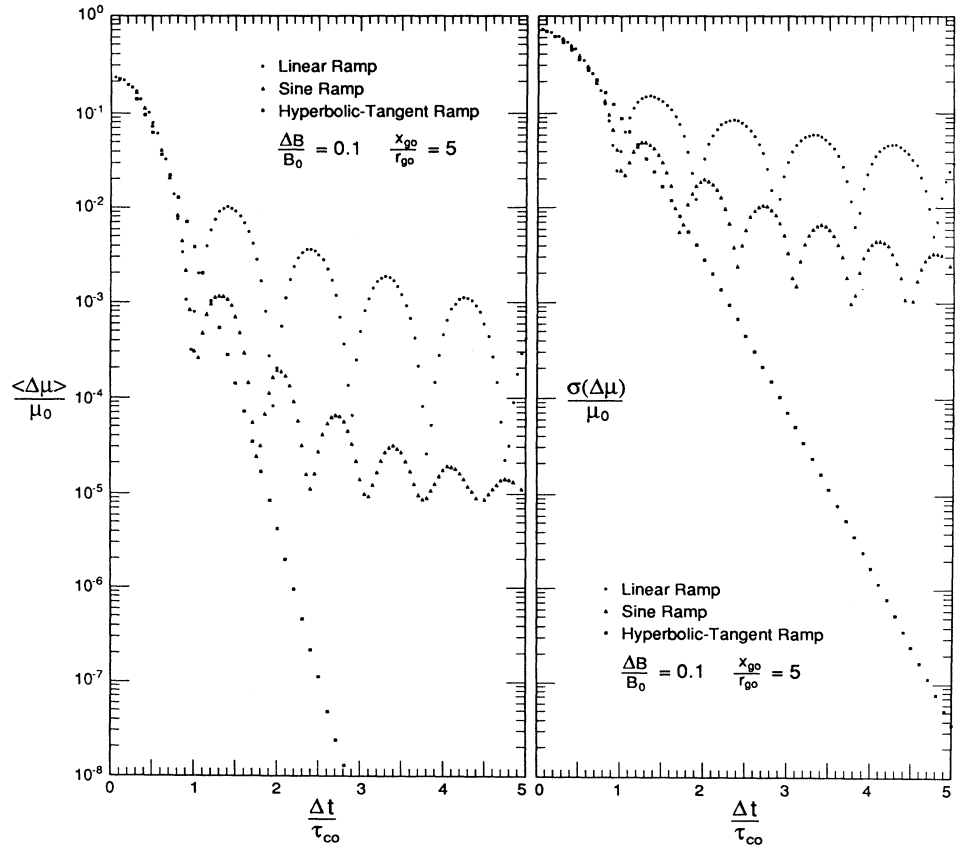

FIG. 15. For the three ramp functions of Fig. 14, the ensemble quantities $\langle \Delta\mu \rangle/\mu_0$ (left panel) and $\sigma(\Delta\mu)/\mu_0$ (right panel) are plotted as functions of the ramp length Δt.

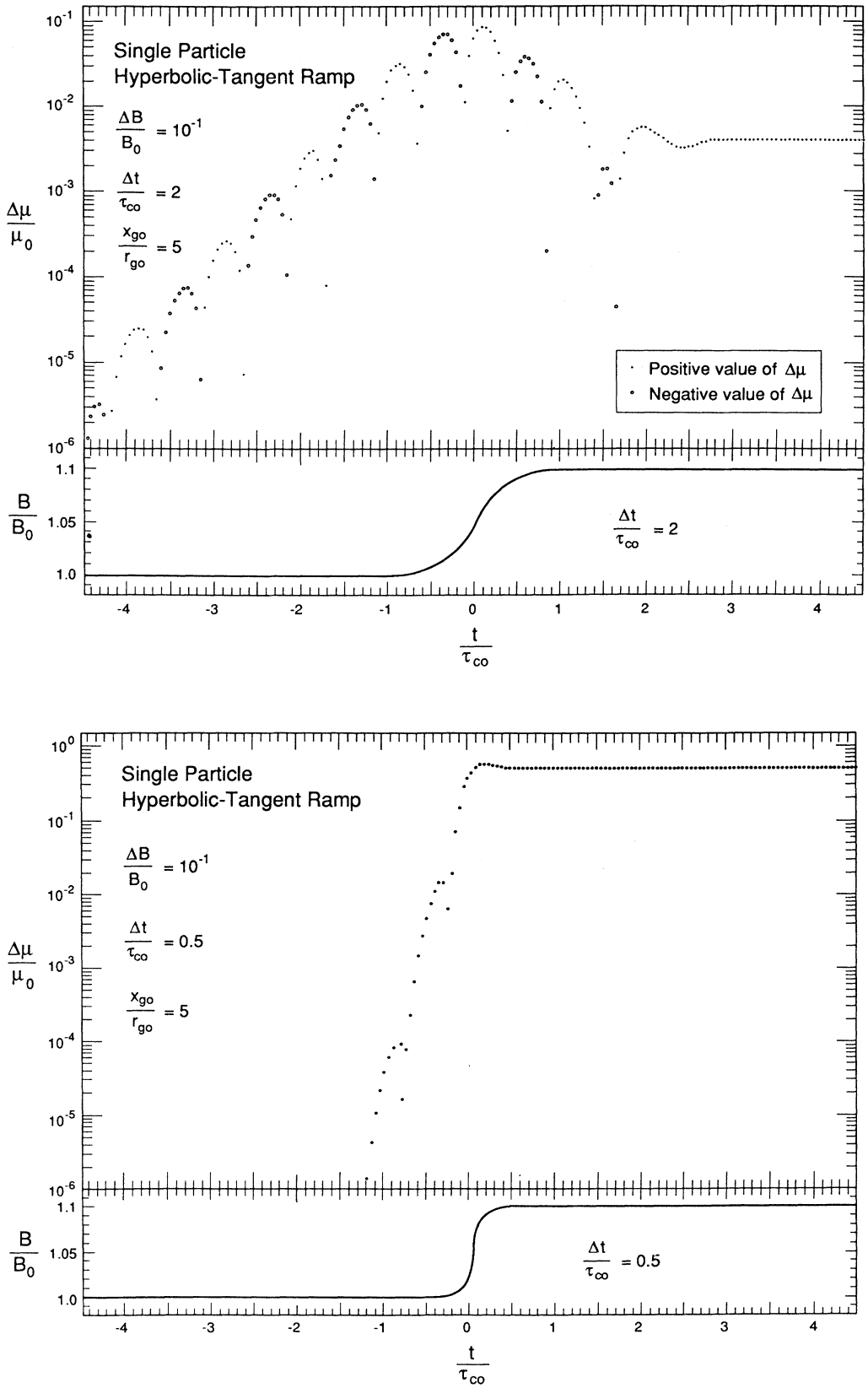

FIG. 16. For a slower (top panels) and a faster (bottom panels) hyperbolic-tangent ramp, the $\Delta\mu/\mu_0$ value for a single particle is plotted as a function of time.

$$\frac{\langle \Delta\mu \rangle}{\mu_0} \approx 1.24 \left[\frac{\Delta B}{B_0} \right]^2 \left[\frac{x_{g0}}{r_{g0}} \right]^0 e^{-7.3\Delta t/\tau_{c0}}, \quad (48a)$$

$$\frac{\sigma(\Delta\mu)}{\mu_0} \approx 0.13 \left[\frac{|\Delta B|}{B_0} \right]^1 \left[\frac{x_{g0}}{r_{g0}} \right]^0 e^{-3.8\Delta t/\tau_{c0}} \quad (48b)$$

for $x_{g0}/r_{g0} \ll 1$.

VI. DISCUSSION OF THE LITERATURE

For a charged particle in a time-changing magnetic induction, $\Delta\mu$ can be larger than would be expected from an examination of the literature on the first adiabatic invariant. This unexpected largeness stems from two properties: (i) $\Delta\mu$ depends on the position of the particle and (ii) the particle might not complete an integer number of gyro-orbits during the magnetic-induction change. The position dependence of $\Delta\mu$ leads to an extra criterion that must be satisfied in order for $\Delta\mu$ to be small [Eq. (5)]. In textbooks (for example, Refs. 4, 7, 16, 17, 20, and 33), as in most of the literature, it is commonly stated that μ is conserved provided that the time variation of B is slow and that spatial gradients in the electromagnetic fields are weak; there is typically no mention of the spatial dependence of $\Delta\mu$, let alone that there is a restriction on the spatial location of a particle if $\Delta\mu$ is to be kept small. A prominent exception to this is the work of Hertweck and Schluter,[28] wherein it is pointed out that $\Delta\mu$ is larger for particles far out from the point where the induction electric field vanishes than for particles at the point where it vanishes.

The case where the magnetic-induction-change time Δt is an exact integer number number of gyroperiods is generally the only case considered in the literature. The probability that a time Δt is exactly equal to an integer times τ_c is small, therefore considering cases where the gyro-orbits are incomplete is important. Two exceptions to the generality are Landau and Lifshitz,[15] wherein it is mentioned that $\Delta\mu$ can be finite if the action integrals are incomplete, and, again Hertweck and Schluter,[28] wherein the case of an incomplete gyro-orbit is analyzed. Hertweck and Schluter (whose work is repeated in Ref. 34) analyzed cases where the magnetic induction changes very quickly (see Sec. III C for a comparison of their results to the present results) and cases where the magnetic

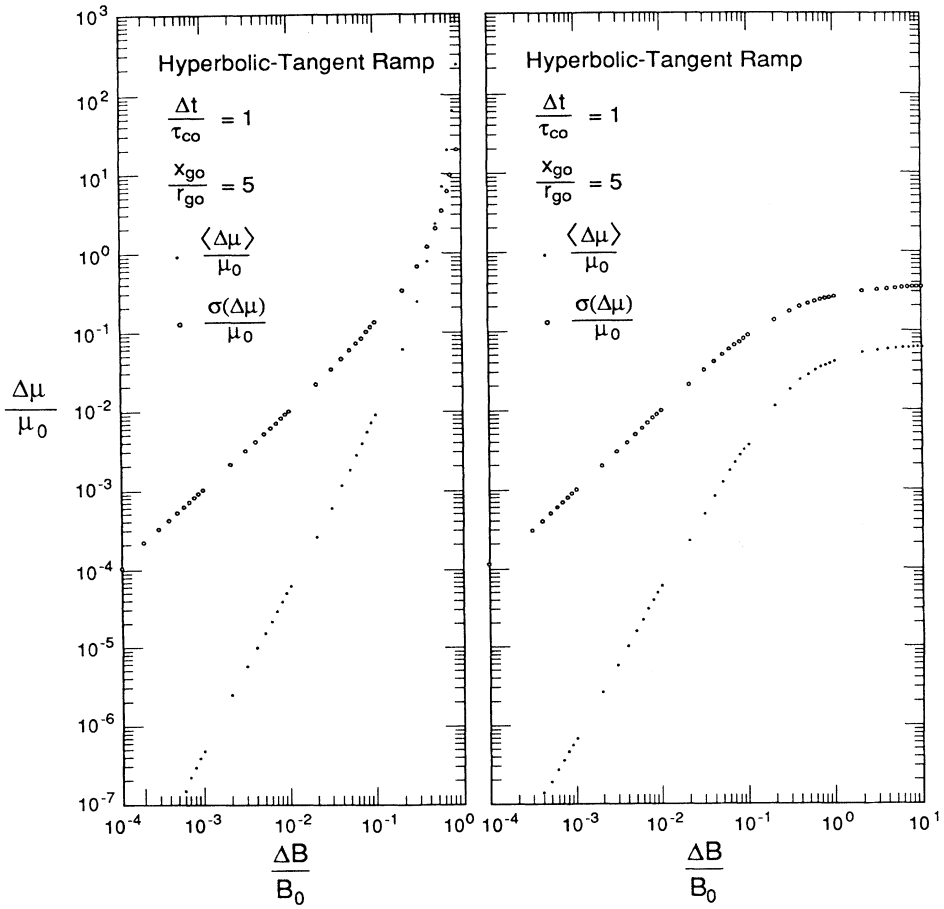

FIG. 17. For test particles that have passed through hyperbolic-tangent ramps with fixed Δt values and with x_{g0} values fixed, the ensemble quantities $\langle \Delta\mu \rangle / \mu_0$ and $\sigma(\Delta\mu)/\mu_0$ are plotted as functions of the change in B across the ramp. The left-hand panel is for B decreasing across the ramps, and the right-hand panel is for B increasing across the ramps.

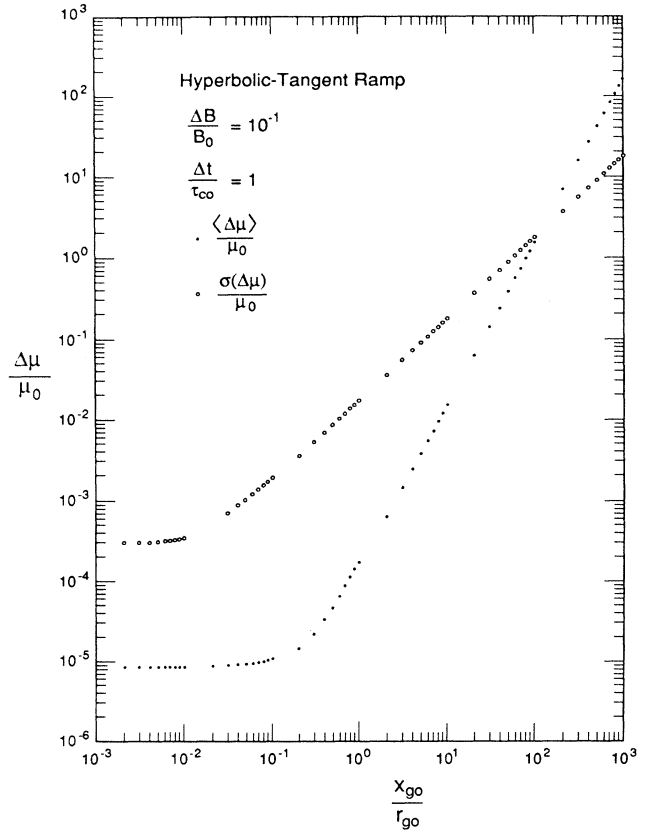

FIG. 18. For hyperbolic-tangent ramps with fixed values of ΔB and Δt, the quantities $\langle \Delta\mu \rangle / \mu_0$ and $\sigma(\Delta\mu)/\mu_0$ are plotted as functions of the initial position x_{g0} of the ensemble guiding centers.

induction changes with time with a hyperbolic-tangent function (see Sec. V for a discussion of those results).

Besides the present work, the authors are aware of only two other studies that have used numerical simulations to investigate the breaking of adiabatic invariants in time-dependent systems, although there have been several computational studies to determine $\Delta\mu$ for particles orbiting in time-stationary magnetic fields.[35–40] The two studies for time-dependent systems are those of Hertweck and Schluter[28] (for hyperbolic-tangent functions) and of Howard[41] (for Gaussian functions). The numerical work of Hertweck and Schluter has pertinence to the present work and was discussed in Sec. V, where favorable comparisons with theory for the particular time dependences were made.

For laboratory devices with time-stationary magnetic fields, data exist on the behavior of charged particles that can be compared with theoretical predictions for $\Delta\mu$ values for these time-stationary fields.[38,42–49] One experiment[46] studied the behavior of mirroring particles in the presence of an imposed, time-dependent electrostatic field. However, no published data for particles in time-dependent magnetic fields have been found. Data pertinent to the breaking of μ do exist for electrons and ions injected into the Earth's magnetosphere by nuclear explosions,[50–52] for electrons and ions injected into the Earth's magnetosphere by magnetic storms,[53,54] and for electrons and ions absorbed by moons in the magnetospheres of Jupiter and Saturn.[55,56] For magnetospheric particles, the dominant causes of the change in μ are Coulomb scattering of atmospheric gases and resonant interactions with electromagnetic plasma waves. Because the amplitudes of plasma waves in the magnetospheres are not well known, the observed time scales for the evolutions of magnetospheric particle distributions are used to infer the time dependences of the magnetospheric fields, rather than the particle data being used as a test of theoretical predictions for the breaking of μ.

VII. SUMMARY

Test-particle computer simulations and analytic theory were used to investigate the first adiabatic invariant μ for charged particles moving in spatially uniform, temporally varying magnetic fields. The fractional change $\Delta\mu/\mu_0$ that resulted from a change in the magnetic induction was examined, and expressions for the statistical quantities $\langle \Delta\mu \rangle / \mu_0$ and $\sigma(\Delta\mu)/\mu_0$ were obtained as functions of the magnetic-induction parameters and the initial conditions of the particles.

A picture for the quantity $\Delta\mu$ based upon the unbalanced work done by the induction electric field on particles undergoing cyclotron motion was presented. Agreement was found between the computer-simulation data and the analytic calculations. This agreement confirmed some physical pictures upon which the breaking of μ is explained.

Large oscillations in $\Delta\mu/\mu_0$ versus Δt (the time over which the magnetic induction changes) were seen. These oscillations stem from fundamental differences between cases when Δt is exactly equal to integer numbers of gyroperiods (complete action integrals) and when Δt is not exactly equal to integer numbers of gyroperiods (incomplete action integrals). The quantity $\mu = v_\perp^2/B$ was found to be an adiabatic invariant even when the action integrals were incomplete. The statistical quantities $\langle \Delta\mu \rangle / \mu_0$ and $\sigma(\Delta\mu)/\mu_0$ are found to follow simple scaling relations with $\Delta B/B_0$, $\Delta t/\tau_{c0}$, and x_{g0}/r_{g0}. These scaling relations were found to hold even for $\Delta B/B_0$ not small and $\Delta t/\tau_{c0}$ not big. Thus, the scalings hold even outside of the adiabatic limit of parameter space. A new criterion for keeping $\Delta\mu$ small was presented, this criterion limiting the magnitude of x_{g0}/r_{g0}.

The behavior of the first adiabatic invariant was examined for magnetic fields that underwent changes in strength through three different types of temporal functions. For changes that occur over brief time intervals, the resulting changes $\Delta\mu$ are insensitive to the functional form that describes the change in B. For changes that occur very slowly, the resulting changes $\Delta\mu$ are very sensitive to the functional form of $B(t)$.

ACKNOWLEDGMENTS

This work was supported at Los Alamos National Laboratory by the U.S. Department of Energy and by the NASA Research and Analysis Program under Contract No. W-17003, and at the University of Iowa by NASA Grant Nos. NSG-7632 and NAGW-970 and by NSF Grant No. ATM-8712236. One of the authors (J.E.B.) wishes to thank KMS Fusion for their hospitality during part of this work.

[1]H. Alfvén, Ark. Mat. Astron. Fys. **27A**, 22 (1940).
[2]P. Ehrenfest, Proc. Amsterdam Acad. **19**, 576 (1916).
[3]T. J. M. Boyd and J. J. Sanderson, *Plasma Dynamics* (Barnes & Noble, New York, 1969), Sec. 2.7.
[4]D. R. Nicholson, *Introduction to Plasma Theory* (Wiley, New York, 1983), Sec. 2.7.
[5]B. Rossi and S. Olbert, *Introduction to the Physics of Space* (McGraw-Hill, New York, 1970), Sec. 5.8.
[6]L. R. Lyons and D. J. Williams, *Quantitative Aspects of Magnetospheric Physics* (Reidel, Dordrecht, 1984), Chaps. 3 and 4.
[7]S. A. Kaplan and S. B. Pikelner, *The Interstellar Medium* (Harvard Univesity, Cambridge, MA, 1970), Sec. 17.
[8]M. S. Longair, *High Energy Astrophysics* (Cambridge University Press, London, 1981), Sec. 13.1.3.
[9]W. F. G. Swann, Phys. Rev. **43**, 217 (1933).
[10]W. F. G. Swann, J. Franklin Inst. **258**, 383 (1954).
[11]P. Ehrenfest, Proc. Amsterdam Acad. **16**, 591 (1913).
[12]P. O. Vandervoort, Ann. Phys. **10**, 401 (1960), Sec. 11.
[13]A. Lenard, Ann. Phys. **6**, 261 (1959).
[14]R. M. Kulsrud, Phys. Rev. **106**, 205 (1957).
[15]L. D. Landau and E. M. Lifshitz, *Mechanics* (Pergamon, Oxford, England, 1960), Sec. 51.
[16]H. Goldstein, *Classical Mechanics,* 2nd ed. (Addison-Wesley, New York, 1981), Sec. 11-7.
[17]J. D. Jackson, *Classical Electrodynamics,* 2nd ed. (Wiley, New York, 1975), Sec. 12.6.
[18]M. Kruskal, in *Plasma Physics,* edited by B. B. Kadomtsev, M. N. Rosenbluth, and W. B. Thompson (International Atomic Energy Agency, Vienna, 1965), p. 91.
[19]T. G. Northrop, *The Adiabatic Motion of Charged Particles* (Wiley, New York, 1963).
[20]H. Alfvén and C.-G. Falthammar, *Cosmic Electrodynamics,* 2nd ed. (Oxford University Press, Cambridge, England, 1963), Sec. 2.2.1.
[21]G. Schmidt, Phys. Fluids **5**, 994 (1962).
[22]J. E. Borovsky and P. H. Hansen (unpublished).
[23]N. A. Krall and A. W. Trivelpiece, *Principles of Plasma Physics* (McGraw-Hill, New York, 1973), Sec. I.3.2.
[24]C. L. Longmire, *Elementary Plasma Physics* (Interscience, New York, 1963), Sec. 2.7.
[25]L. Spitzer, Jr., *Physics of Fully Ionized Gases* (Interscience, New York, 1962), Sec. 1.3.
[26]J. L. Shohet, *The Plasma State* (Academic, New York, 1971), Sec. 5.A.
[27]J. G. Roederer, *Dynamics of Geomagnetically Trapped Radiation* (Springer-Verlag, Berlin, 1970), Sec. I.6.
[28]F. Hertweck and A. Schluter, Z. Naturforsch. **12A**, 844 (1957).
[29]G. N. Watson, *Theory of Bessel Functions* (Cambridge University Press, Cambridge, England 1952).
[30]*Handbook of Mathematical Functions,* Appl. Math. Ser. No. **55**, edited by M. Abramowitz and I. A. Stegun (U.S. GPO, Nat. Bur. Stand. Washington, DC, 1964).
[31]G. Backus, A. Lenard, and R. Kulsrud, Z. Naturforsch. **15A**, 1007 (1960).
[32]L. J. F. Broer and L. van Wijngaarden, Appl. Sci. Res. B **8**, 159 (1960).
[33]B. Lehnert, *Dynamics of Charged Particles* (Elsevier, New York, 1964), Table 4.1.
[34]S. Chandrasekhar, *Plasma Physics* (University of Chicago, Chicago, 1960), Chap. III.
[35]J. E. Howard, Phys. Fluids **14**, 2378 (1971).
[36]A. J. Dragt, Rev. Geophys. **3**, 255 (1965).
[37]J. E. Howard, Phys. Fluids **11**, 1569 (1968).
[38]J. H. Foote, Plasma Phys. **14**, 543 (1972).
[39]R. H. Cohen, G. Rowlands, and J. H. Foote, Phys. Fluids **21**, 627 (1978).
[40]E. C. Whippel, T. G. Northrop, and T. J. Birmingham, J. Geophys. Res. **91**, 4149 (1986).
[41]J. E. Howard, Phys. Fluids **13**, 2407 (1970).
[42]G. Gibson, W. C. Jordan, and E. J. Lauer, Phys. Fluids **6**, 116 (1963).
[43]G. Gibson, W. C. Jordan, and E. J. Lauer, Phys. Fluids **6**, 133 (1963).
[44]G. Gibson, W. C. Jordan, and E. J. Lauer, Phys. Rev. Lett. **5**, 141 (1960).
[45]J. R. Roth, Phys. Fluids **6**, 2538 (1966).
[46]A. N. Dubinina, L. A. Trainin, and D. V. Chirikov, Zh. Eksp. Teor. Fiz. **49**, 373 (1965) [Sov. Phys.—JETP **22**, 260 (1966)].
[47]A. N. Dubinina and L. S. Krasitskaya, Pisima Zh. Eksp. Teor. Fiz. **5**, 230 (1967) [JETP Lett. **5**, 184 (1967)].
[48]A. N. Dubinina and Y. N. Yudin, Zh. Eksp. Teor. Fiz. **53**, 1206 (1967) [Sov. Phys.—JETP **26**, 707 (1968)].
[49]A. N. Dubinina, L. S. Krasitskaya, and Y. N. Yudin, Plasma Phys. **11**, 551 (1969).
[50]M. Walt and L. L. Newkirk, in *Space Research V,* edited by D. G. King-Hele, P. Muller, and G. Righini (North-Holland, Amsterdam, 1965), p. 458.
[51]R. C. Filz and E. Holeman, J. Geophys. Res. **70**, 5807 (1965).
[52]R. S. White, Phys. Today **19** (10), 25 (1966).
[53]A. Rosen and N. L. Sander, J. Geophys. Res. **76**, 110 (1971).
[54]L. J. Lanzerotti, C. G. Maclennan, and M. F. Robbins, J. Geophys. Res. **76**, 259 (1971).
[55]A. W. Schardt and C. K. Goertz, in *Physics of the Jovian Magnetosphere,* edited by A. J. Dessler (Cambridge University Press, Cambridge, England, 1983), p. 157.
[56]J. A. Van Allen, in *Saturn,* edited by T. Gehrels and M. S. Matthews (University of Arizona, Tucson, AZ, 1984), p. 281.